

EFFECT OF CARBON BASED NANOADDITIVES ON EXTERNAL GEAR PUMP PERFORMANCE

BY

PHILIP J. MARTORANA

THESIS

Submitted in partial fulfillment of the requirements  
for the degree of Master of Science in Aerospace Engineering  
in the Graduate College of the  
University of Illinois at Urbana-Champaign, 2011

Urbana, Illinois

Adviser:

Professor Eric Loth

## Abstract

Effect of fine graphite flake, carbon nanotube, and carbon nanofiber additives on the efficiency of an external gear pump driving an ethanol-based closed hydraulic loop was investigated experimentally. A number of graphite, carbon nanotube (CNT) and carbon nanofiber (CNF) dispersions in ethanol were prepared with concentrations ranging from 194-1500 ppm. The fluids were investigated in an external gear pump with a maximum operating pressure of 100 psi. Pump inlet pressure, volumetric flow rate, and electric power consumption data were recorded over a range of pump discharge pressures. The power consumed by the motor at a given differential pump pressure was found to remain approximately constant for all additive concentrations. It was found that increases in both volumetric flow rate and overall pump efficiency were observed when pure ethanol was replaced by the colloidal suspensions. This was attributed to a roller bearing effect caused by the alignment and self-lubrication of the colloidal additives when confined to micro-scale clearances between the gear surfaces. It was found that that pump performance was also a function on the CNT aspect ratio and could vary from pump to pump, or even after a pump was disassembled and reassembled. This indicates that the clearance geometry between the gears and between the housing may play a critical role.

To examine any potential structural changes in the additives, environmental scanning electron microscope (ESEM) images of the additives were obtained before and after extended run periods within the pump. The results indicate that graphite and CNTs retained significant resilience, i.e. no breakage and deformation was observed. However, the very long aspect ratio CNFs appear to have undergone some scission. To examine any issues with filterability,

graphite and CNT suspensions were run through two filters of different size and composition and the filters were then qualitatively examined using ESEM images. The results indicate that a considerable amount of the additives were filtered from the suspension. This indicates that filterability is an issue that needs to be addressed if these suspensions were to be used in industrial applications.

## **Acknowledgements**

I would like to thank God who has given me the ability to complete this research. I would like to thank my advisors Dr. Eric Loth and Dr. Ilker Bayer who have always been extremely kind, understanding, and helpful during the challenging process of completing my Master's degree. I would like to thank the National Science Foundation and the Center for Compact and Efficient Fluid Power whose funding made my research possible. I would also like to thank all the members of my research group for their help. Finally, I would like to thank my mother, father, brother, girlfriend, and all my family and friends whose support and encouragement was instrumental in helping me finish my degree.

## Table of Contents

<b>Chapter 1: Introduction</b> .....	1
<b>1.1 Motivation</b> .....	1
<b>1.2 Previous Studies</b> .....	2
<b>1.3 Objectives</b> .....	2
<b>1.4 Figures</b> .....	5
<b>Chapter 2: Experimental Methods</b> .....	8
<b>2.1 Facility Setup</b> .....	8
<b>2.2 Fluids Tested</b> .....	9
<b>2.3 Imaging</b> .....	11
<b>2.4 Filterability</b> .....	12
<b>2.5 Figures and Tables</b> .....	13
<b>Chapter 3: Results and Discussion</b> .....	19
<b>3.1 Pump One</b> .....	19
<b>3.2 Pump Two</b> .....	23
<b>3.3 Pump Three</b> .....	27
<b>3.4 Pump Four</b> .....	30
<b>3.5 Discussion</b> .....	32
<b>3.6 Figures</b> .....	36
<b>Chapter 4: Conclusions</b> .....	61
<b>References</b> .....	63

## Chapter 1: Introduction

### 1.1 Motivation

Improving the efficiency of liquid pumps is an area of continually increasing importance in the fluid power industry. The overall efficiency of a pump is a combination of two components: the volumetric efficiency and the torque (or mechanical) efficiency. The latter is a measure of the power lost due to fluid shear and internal friction, while the volumetric efficiency is a measure of the power lost due to fluid compressibility and internal leakage [1]. These definitions show that the physicochemical state of the fluid running through a pump is just as important to the efficiency as the physical design of the pump. Viscosity of the hydraulic fluids can play a major role in determining how efficient the pump will perform for a given hydraulic fluid [2]. In fact, viscosity of a hydraulic fluid is a major selection criterion for pump performance. Figure 1 schematically shows the relationship between hydraulic pump fluid viscosity and pump operating conditions and related failure modes. For instance, below 50 mm<sup>2</sup>/s liquid viscosity, reduced equipment life due to high wear rate and overheating is highly probable, whereas above 500 mm<sup>2</sup>/s, sluggish pumping conditions and cavitation along with the formation of uneven lubrication regions inside the pump result [3]. As shown in Figure 2, the volumetric and mechanical efficiencies generally have opposite trends with respect to increasing fluid viscosity. As the fluid viscosity increases, the volumetric efficiency increases due to the reduction in internal leakage, but the mechanical efficiency decreases because more power is required to pump the fluid. Thus, there is an optimum viscosity for which the combined influence of internal leakage and friction losses is minimized so that the overall efficiency of the system will be maximized [4].

## 1.2 Previous Studies

Bielmeier *et al.* [5] examined the effect of the discharge pressure on the volumetric flow rate of a gear pump for two Newtonian oils with different dynamic viscosities. Their results are summarized in Figure 3 with two fluids, where Oil 2 is roughly twice as viscous as Oil 1. They found that flow rate decreased in a linear manner as the discharge pressure was increased. This led them to conclude that the decrease in flow rate was due to an increase in internal leakage, consistent with the trend shown in Figure 2. According to Dearn [6], internal leakage occurs in three specific areas within a gear pump: between the gears themselves, between the gears and the cavity plate, and between the mating surfaces of the gears with the end cap and pump body. If debris and contaminants are contained within the fluid, then over time they may increase internal leakage and reduce volumetric efficiency and pump life as discussed by Jing *et al.* [7]. Thus, in general, presence of particulate matter in the hydraulic fluid is expected to be generally detrimental to pump performance. However, microscopic particles can also have a positive effect on pump performance in the form of additives that modify viscosity, improve lubricity, and prolong hydraulic fluid life. The motivation of this study is an attempt to find particulate matter (i.e. solid microscopic additives) that reduces internal leakage and improves pump performance without changing the bulk viscosity. To the author's knowledge, no such study has previously demonstrated this effect.

## 1.3 Objectives

However, as mentioned earlier, increasing viscosity of the hydraulic fluids results in increased power consumption, sluggish performance, cavitation, and frequent occurrence of poorly lubricated regions within the pump (see Figure 1). Therefore, the design of highly

efficient new water-based and bio-based low viscosity hydraulic fluids has always been at the forefront of the pump industry [3]. This study investigates use of fine graphite flakes, carbon nanotubes of varying aspect ratio, and carbon nanofibers as colloidal additives in a low viscosity fluid (ethanol) corresponding to an operating condition below 5 mm<sup>2</sup>/s hydraulic fluid viscosity as shown in Figure 1.

The additives are used in small enough concentrations (ppm levels) so that the viscosity of the working fluid is not modified at all times. As such, they are not expected to influence the mechanical efficiency. Graphite has been well documented [8-10] as a solid lubricant and more recently has been used to make nanolubricants [11]. In addition, graphite nanofluids have been shown to increase the heat transfer coefficient in flow systems when used as additives [12]. Multi-walled carbon nanotubes, which possess superior mechanical properties [13], of various lengths and diameters were also chosen in order to examine the effect of aspect ratio on the additives' performance. Surface graphitized carbon nanofibers were also chosen since they have unique lubrication properties with additional superior mechanical properties [14]. The latter aspect is important as external gear pumps subject additives to a harsh environment, i.e. high molecular-weight polymers may undergo scission. One may thus expect some improvement in wear with these additives. However, to the author's knowledge, no previous study has shown that use of additives in small concentration (such that viscosity is unaffected) can alter the volumetric efficiency of a pump.

The objective of the study is to investigate the effects of micro/nanoscale carbon-based additives in a closed hydraulic loop. In particular, the effects of different additive concentrations on external gear pump performance are examined. The additives were used as

colloidal suspensions in ethanol with the help of dispersants. Comparisons are presented based on the measured power consumption, measured volumetric flow rates, and calculated overall efficiencies at different concentrations of solid additives (including a base line case with no additives in the closed hydraulic loop). Possible post-run structural changes in the additives were qualitatively analyzed using pre- and post-run environmental scanning electron microscope (ESEM) images of the additives isolated from the colloidal suspensions. The method in which these images were obtained can be found in the imaging section (section 3) of Chapter 2. Certain colloidal suspensions were also run through two filters of different size and material composition to examine the feasibility of using these suspensions in industrial fluid power systems. ESEM images of these filters were also taken. A description of these filters and the process used to obtain the images can be found in the filterability section (section 4) of Chapter 2.

It should be noted that this study is unique in that it is the first to show the use of additives that increase the volumetric efficiency of a gear pump without sacrificing mechanical efficiency (see Figure 2). Other viscosity modifying additives have shown to be effective in increasing the viscosity and volumetric efficiency of a fluid but at the cost of an increase in pump power consumption. In other words, the additives in this study give the working fluid the volumetric efficiency benefits of a higher viscosity fluid without changing the viscosity and lowering the mechanical efficiency of the pump. This is a major breakthrough in this day and age where efficiency is at the forefront of hydraulic product development. The potential use of this novel finding in the fluid power industry could be monumental.

## 1.4 Figures

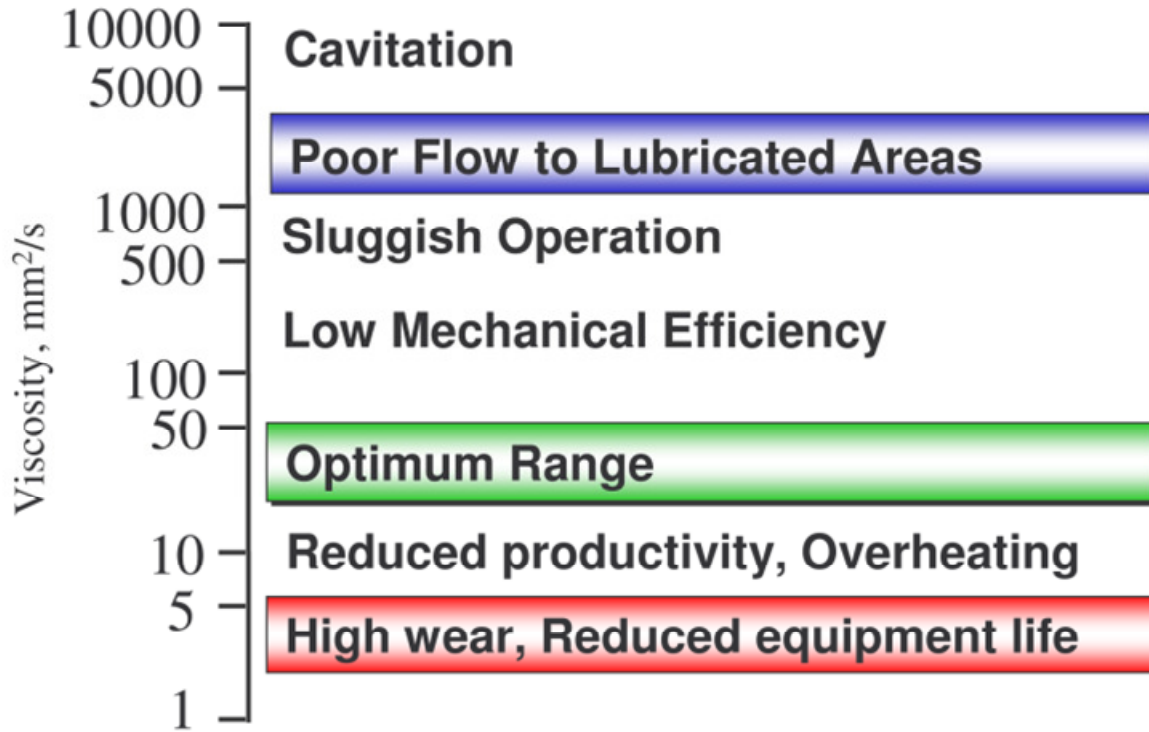


Figure 1. Viscosity dependent operational performance of gear pumps. The hydraulic fluids should be designed to have a viscosity within 20 to 50 mm<sup>2</sup>/s range for optimum pump performance [3].

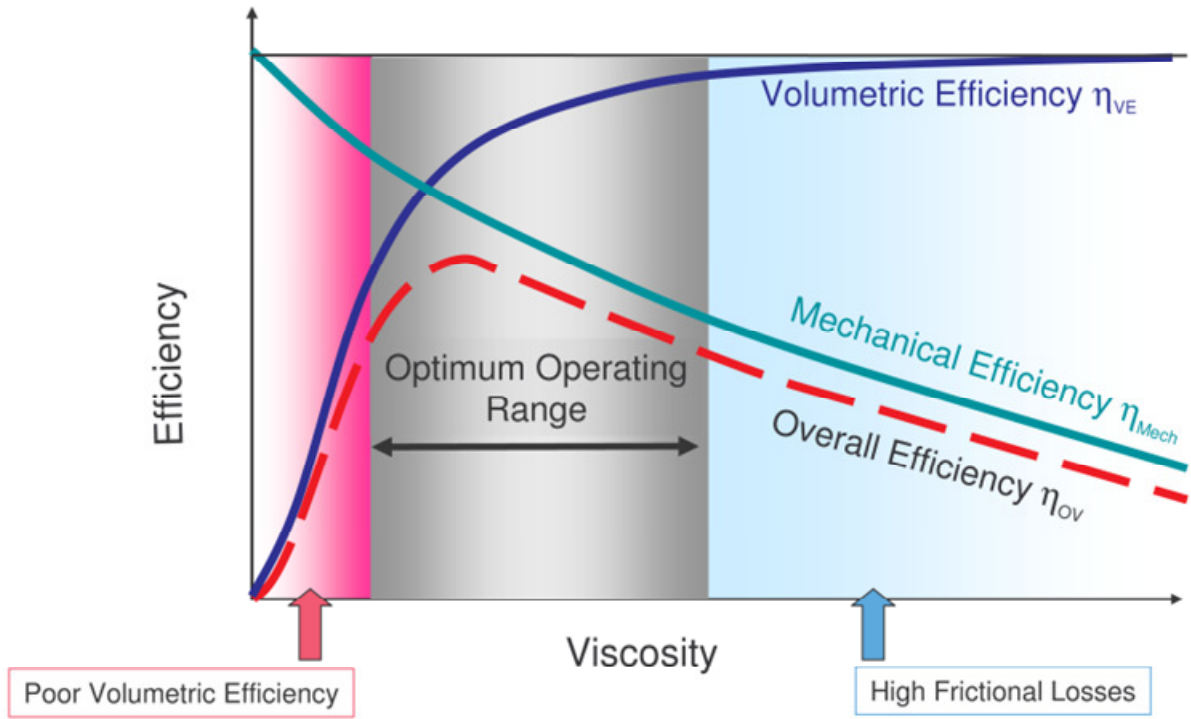


Figure 2. Qualitative representation of the effect of fluid viscosity on the volumetric, mechanical, and overall efficiencies of a gear pump. Reproduced from [4].

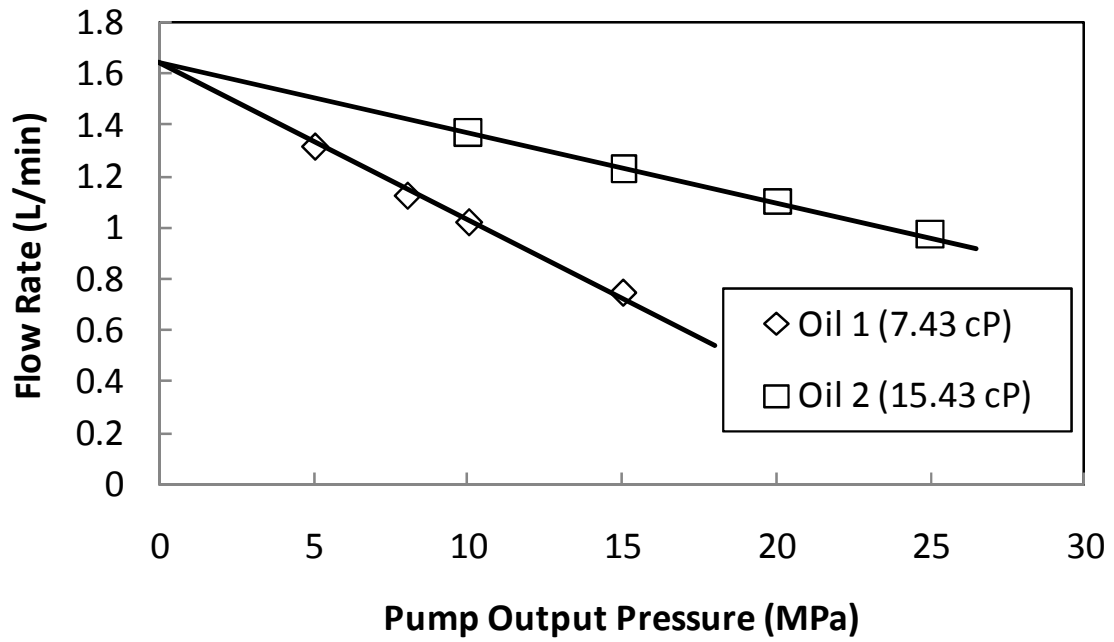


Figure 3. Influence of viscosity on flow rate for a given pump output pressure [5].

## Chapter 2: Experimental Methods

### 2.1 Facility Setup

The closed hydraulic loop experimental setup is shown in Figure 4. A SHURflo (USA) self-priming, positive displacement, external rotary gear pump (McMaster-Carr product number 4272K32) equipped with an internal pressure relief valve drives the hydraulic loop. During the course of these experiments, four SHURflo pumps of the same model were used. The results chapter that follows will be broken down into chronological sections with each pump's experimental results receiving its own section. The pump is driven by a 0.5 horsepower, constant speed (1725 RPM) electrical motor and has 0.25 inch NPT ports and a maximum flow rate of 2.2 GPM (~8.3 LPM). The digital vacuum gauge at the intake port has a range of 0 to 30 inches Hg (referenced to ambient pressure), and the digital pressure gauge at the discharge port has a range of 0 to 100 psig. Two different flow meters were used throughout the course of the research (both attached downstream of the discharge port). One is an analog volumetric flow meter from Omega with a range of 1-7.5 LPM, and the other is a digital volumetric flow meter from Assured Automation with a range of 1-30 LPM. Each results section will indicate which flow meter was used. A pre-calibrated power meter was used to measure the electrical power consumed by the motor. Additional information about the instrumentation used can be found in Table 1. The discharge pressure was manipulated by using a Deltrol Fluid Products needle valve installed downstream of the discharge port and/or the internal pressure relief valve of the pump. Each results section will indicate the specific method used to manipulate the pressure. The experiments were designed so that a baseline case of pure ethanol was run first. The different concentrations of graphite, CNT, or CNF suspensions were then run in order

of increasing concentration (starting with the lowest). At the end of each run, a water-based cleaning solution and pure ethanol were run successively several times through the hydraulic loop to ensure that particulate residues and debris from the previous runs were flushed out of the system completely. The manner in which these experiments were performed evolved as the research progressed. Specific details of how each experiment was carried out will be given in its corresponding pump section in the results and discussion chapter (Chapter 3).

## **2.2 Fluids Tested**

In the beginning stages of this study, various fluids were tested in order to gain insight into the behavior of the pump. These initial fluids tested were tap water, ethanol, mineral oil, and a crude oil which contained the polymer heptane. The results from the tap water, ethanol, and mineral oil provided baseline data with which to compare to data obtained from future tests using colloidal suspensions. The results from the crude oil with heptane provided an example of an additive that did not improve pump efficiency and appeared to actually lessen it. Ethanol was chosen as the primary fluid to use for creating the colloidal suspensions because of the results obtained from these initial experiments (which are discussed in Chapter 3.1), along with the facts that it was readily available, affordable, and the easiest of the initial fluids tested with which to obtain good dispersion of additives.

Graphite was the first carbon-based additive to be examined. The colloidal graphite stock used in this work was a 22 wt. % graphite flake (density =  $2.26 \text{ g/cm}^3$ , 99+% fixed carbon) dispersion with an average particle size of 0.8–2.0  $\mu\text{m}$  in 200 proof ethanol (Grafo Hydrograf A M2 from Fuchs Lubricant, USA). The suspension contains cellulose acetate as binder and

dispersant. As received graphite stock was diluted with ethanol to obtain four different concentrations (1550, 775, 388, and 194 ppm) of colloidal suspensions.

Multi-walled carbon nanotubes were the next micro/nanoscale additive to be examined. The initial type of CNT used was from Sigma Aldrich and had a diameter of 110-170 nanometers and a length of 5-9 microns. Colloidal suspensions of 200, 400, 600, and 1000 ppm were created with these CNTs. The surfactant silyl-terminated polyether was added to these mixtures in a concentration which did not exceed 1 wt. % in order to help with dispersion. In order to examine the effect of aspect ratio (length divided by width) on pump behavior two additional types of CNTs were also examined. They both were from NanoAmor and had a diameter of 50-80 nm. One type had a length of 0.5-2.0  $\mu\text{m}$  while the other had a length of 10-20  $\mu\text{m}$ . Initially, these CNTs were separately dispersed in ethanol with the help of the surfactant SDS, the concentration of which did not exceed 1 wt. %. The CNT-ethanol/surfactant mixtures were sonicated for two hours using a Sonics VCX 750 ultrasonic processor to form two stable CNT suspensions of 500 and 1000 ppm for each type of CNT. The information about the CNTs used in this study is summarized in Table 2.

The final additives studied were carbon nanofibers. Highly graphitic, Pyrograf-III, carbon nanofibers were obtained from Applied Sciences Inc. (Dayton, OH, USA). The CNFs are vapor-grown PR-24-XT PS grade fibers which were fabricated by pyrolytic stripping of the as-grown fibers to remove polyaromatic hydrocarbon residues of the synthesis process from the nanofiber surface. This surface stripping takes place at around 600 °C without altering the existing carbon nanofiber microstructure. Initially, the CNFs were dispersed in ethanol with the help of the surfactant SDS, the concentration of which did not exceed 1 wt. %. The CNF-

ethanol/surfactant mixtures were sonicated for two hours using a Sonics VCX 750 ultrasonic processor to form four stable CNF suspensions of 200, 400, 800 and 1600 ppm. The experimental results for all the different colloidal suspensions can be found and are discussed in Chapter 3.

As previously mentioned, this study aims to use the additives in small enough amounts so that the viscosity of the fluid remains unchanged. Figure 5 shows the dynamic viscosity of the graphite, CNT, and CNF colloidal dispersions in ethanol as a function of concentration. The viscosity of the mineral oil that was tested is also shown for reference. The measurements were conducted using a Brookfield DV-II+PRO desktop viscometer. The additives did not change the viscosity of ethanol for the concentrations studied as shown in Figure 5. This assures that any changes seen in pump performance as a result of replacing pure ethanol with graphite, CNT, and/or CNF colloidal suspensions are not related to viscous effects.

### **2.3 Imaging**

In order to examine the effect of the confined environment of the gear pump on the structural integrity of the nanoadditives, ESEM images of the additives were taken both before and after the experiments were run. The suspension containing the additive to be imaged was first sonicated until a good dispersion was obtained. An eye dropper was then used to take a small amount of the suspension and deposit it onto a glass microscope slide. This slide was allowed to dry overnight so that the ethanol evaporated. The nanoadditive (along with some surfactant) that was deposited on this slide could then be imaged using an ESEM. This process was done for each type of nanoadditive using the highest concentration to ensure a sufficient

amount of the additive was deposited on the glass slide. These images can be found and are discussed in Chapter 3.

## **2.4 Filterability**

Two different filters were tested in the closed hydraulic loop in order to examine how they affected the suspensions. The first filter that was used in the hydraulic loop was produced by the Pall Corporation. It was a Claris Series filter composed of high consistency polypropylene. It had a nominal rating of 30  $\mu\text{m}$ . This filter can be seen in Figure 6. It was contained in a LMO Series filter housing made of carbon steel. After running the suspension through the filter, it was taken from its housing and a small portion of it was then removed using scissors in order to obtain ESEM images. The second filter used in the hydraulic loop was produced by McMaster-Carr. It was a mesh screen comprised of Type 304 stainless steel housed in a bronze  $\gamma$ -strainer. It had a nominal rating of 75  $\mu\text{m}$ . This filter can be seen in Figure 7. The mesh screen was removed from its housing and then cut using scissors so that it could be laid flat for ESEM imaging. These filters were chosen because they allowed observations to be made about how both filter composition and rating affect the suspensions. These images can be found and are discussed in Section 2 of Chapter 3.

## 2.5 Figures and Tables

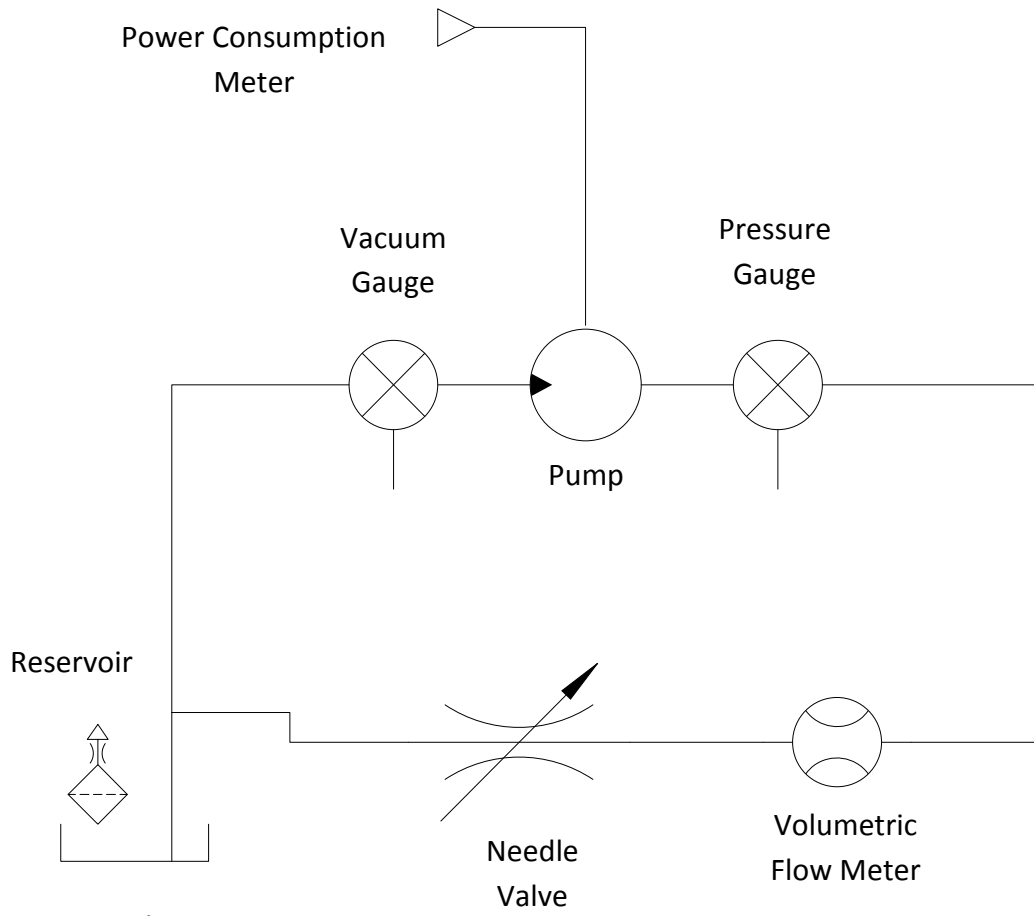


Figure 4. Facility setup.

Table 1. Instrument data.

Instrument	Manufacturer	Range	Accuracy
Pressure gauge (vacuum)	Omega	0-30 in Hg	±0.25% of full scale
Pressure gauge	Omega	0-100 psig	±0.25% of full scale
Volumetric flow meter	Omega	1-7.5 LPM	±2.0% of full scale
	Assured Automation	1-30 LPM	±0.5%
Power meter	Optimum Energy Products	0-1875 W	±0.5%-2.0%

Table 2. Different CNTs tested in closed hydraulic loop.

Type	Manufacturer	Diameter	Length	Aspect Ratio
Multi-walled	Sigma Aldrich	110-170 nm	5-9 $\mu\text{m}$	45-53
Multi-walled	NanoAmor	50-80 nm	0.5-2.0 $\mu\text{m}$	10-25
Multi-walled	NanoAmor	50-80 nm	10-20 $\mu\text{m}$	200-250

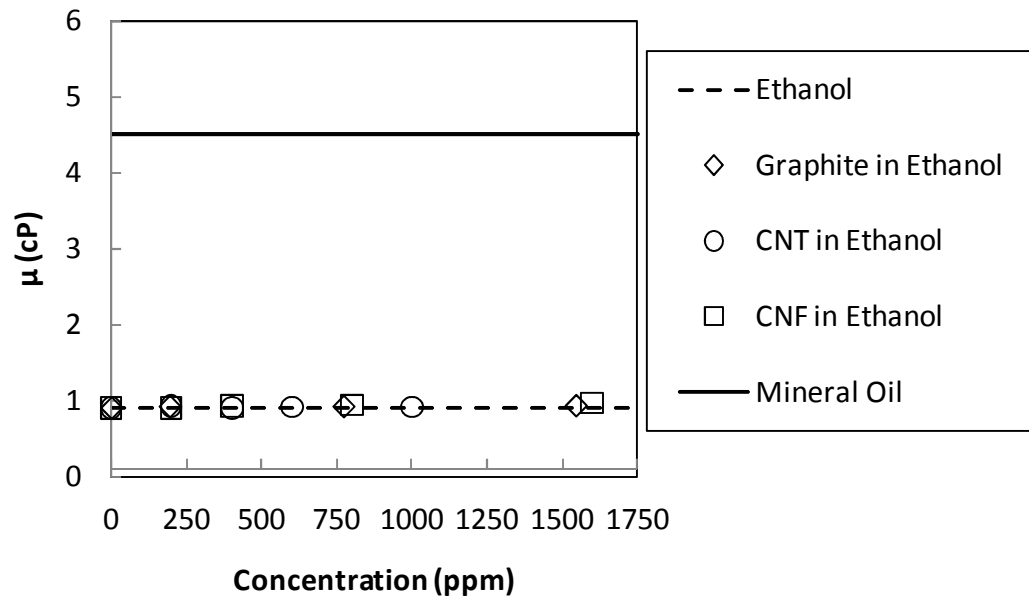


Figure 5. Dynamic viscosity for different fluids and additive concentrations.



Figure 6. Claris Series filter from the Pall Corporation.



Figure 7. Mesh screen filter from McMaster-Carr.

## Chapter 3: Results and Discussion

### 3.1 Pump One

In order to gain an understanding of how the pump behaved four different fluids were initially tested. As previously mentioned, these four fluids were tap water, ethanol, mineral oil, and a crude oil containing the polymer heptane. The fluid to be tested was poured into a plastic reservoir which contained the intake and discharge tubing of the system. The pump was turned on with the internal pressure relief valve completely closed and the needle valve completely open. The needle valve was closed in a manner so that the discharge pressure increased in approximately 5 psi intervals. At each of these intervals, the inlet pressure, discharge pressure, volumetric flow rate (obtained from the Omega volumetric flow meter for these experiments), and power consumption data was recorded. These values were used to calculate overall pump efficiency. Power into the system was assumed to be equal to half the value recorded off the power consumption meter as recommended by the pump and motor manufacturer. The power output by the pump was calculated by multiplying the volumetric flow rate by  $\Delta p$  across the pump. Differential pressure or  $\Delta p$  is defined as the absolute pressure difference between the reading from the pressure gauge on the discharge side of the pump and the reading from the vacuum gauge on the inlet side of the pump (refer to Figure 4).

This data was used to produce Figures 8-10. Figure 8 shows the power supplied to the motor as function of differential pressure ( $\Delta p$ ) across the pump. The pump required approximately the same amount of power to move all of the fluids for a given differential pressure with the exception of the crude oil and heptane at high end of the  $\Delta p$  region. Figure 9 shows the volumetric flow rate as a function of differential pressure across the pump. The

crude oil with heptane had the lowest flow rate for a given  $\Delta p$  while ethanol had the highest with the exception of a few points at the high end of the  $\Delta p$  region, where mineral oil had the highest flow rate. Figure 10 shows overall efficiency as a function of differential pressure across the pump. Once again, the crude oil with heptane had the lowest overall efficiency for a given  $\Delta p$  while ethanol had the highest with the exception of a few points at the high end of the  $\Delta p$  region, where mineral oil had the highest efficiency. One reason why ethanol was chosen as the fluid used to create the colloidal suspensions was because the pump generally performed the best overall with ethanol as the working fluid. In other words, it would not make sense (from both an intellectual and financial viewpoint) to try and improve the performance of the pump by using additives in tap water when you could simply use ethanol instead. The pump performing better in the higher  $\Delta p$  region with mineral oil as the working fluid could be a viscous effect as exemplified in Figure 3. Through the use of additives (in small enough amounts so as not to change the fluid's viscosity), perhaps a colloidal suspension made with ethanol could maintain its good performance at low  $\Delta p$  while matching or surpassing the performance of the mineral oil at high  $\Delta p$ . In other words, the colloidal suspension would gain the volumetric benefits of a higher viscosity fluid without sacrificing mechanical efficiency. This was another reason why ethanol was chosen as the fluid used to create the suspensions.

The ethanol and graphite colloidal suspensions were the first to be prepared and tested. The graphite stock was added to a plastic reservoir filled with a premeasured amount of ethanol. The mixture was then mechanically shaken until good dispersion was obtained. This process was used to create four different concentrations (1550, 775, 388, and 195 ppm) of the graphite-ethanol colloidal suspensions. The suspensions were always mechanically shaken

prior to testing. Also, the system was allowed to run for at least five minutes before any pressure manipulation was performed which further helped to ensure proper mixing and good additive dispersion. The suspensions were tested in order of increasing concentration (i.e. pure ethanol first and the highest concentration last). The pump was turned on with both the internal pressure relief valve and needle valve completely open. The relief valve was left open in order to obtain a wider range of pressures tested. The internal relief valve was then tightened so that the discharge pressure increased in increments of 2-10 psi (it is difficult to obtain precise pressure adjustments using the internal relief valve). Once the internal relief valve was tightened completely, the needle valve was closed in a manner so that the discharge pressure continued to increase in 5-10 psi intervals. At each of these intervals, the inlet pressure, discharge pressure, volumetric flow rate (obtained from the Omega volumetric flow meter for these experiments), and power consumption data was recorded. After an experiment with a particular suspension was completed, the system was drained, flushed numerous times with pure ethanol, and allowed to dry before the next solution was tested.

This data was used to produce Figures 11-13. To assess the additive performance on mechanical efficiency, the power consumption of the pump was recorded as a function of differential pressure across the pump. The results for pure ethanol and for the graphite colloidal suspensions can be seen in Figure 11. The results indicate a linear increase in power as the differential pressure across the pump increases, consistent with theoretical trends. Note that for a given pressure drop across the pump, no change in pump power consumption was observed as a function of graphite concentration compared to pure ethanol. In other words, the power required at a given  $\Delta p$  is essentially independent of additive concentration.

Therefore, changes in mechanical efficiency due to possible hydraulic fluid viscosity changes can be ruled out. Figure 12 shows volumetric flow rate change as a function of differential pressure across the pump for selected graphite colloidal fluids. This data was plotted to explore the dependence of maximum volumetric flow rate at a given  $\Delta p$  on additive concentration. It appears that the first part of the data points contradict those obtained by Bielmeier et al. in Figure 3. However, this can be explained by the use of the internal pressure relief valve in initially raising the pressure. The relief valve is designed to temporarily allow fluid to flow from the discharge side of the pump back into the inlet side of the pump when the discharge pressure reaches a certain critical pressure. This critical pressure could be set by the relief valve to a low or high value depending on the desired operation. At the beginning of each experiment the relief valve was not set to full strength, thus maintaining a low discharge pressure and allowing a large amount of backflow within the pump. Tightening the internal relief valve (i.e. raising the critical pressure) effectively reduces the internal leakage in the pump which explains the initial rise in flow rate as pressure is increased. The transition between using the internal relief valve and the needle valve corresponds to the data points in Figure 12 where the flow rate remains approximately constant as pressure increases. As Figure 12 shows, as the additive concentration is increased the volumetric flow rate increases for a given  $\Delta p$ . Though the 388ppm, 775 ppm, and 1550 ppm graphite concentrations of Figure 12 produce similar volumetric flow rates for a given  $\Delta p$ , they still produce increases in flow rate over the 194 ppm graphite concentration and pure ethanol. These results suggest a reduction in internal pump leakage. Figure 13 shows overall efficiency as a function of differential pressure across the pump for the different suspensions and pure ethanol. The overall efficiency

was calculated as the power output by the pump divided by the power input to the pump by the motor. The power output by the pump was found by multiplying the flow rate by the discharge pressure [1]. The electrical motor used was a 50% efficient motor as indicated by the manufacturer's specifications. Thus the measured power of the motor was divided by 2 in calculating the power input to the pump by the motor. At lower differential pressures, the additives can be seen to improve pump efficiency. However, this effect diminishes as  $\Delta p$  increases and at the high end of the  $\Delta p$  region the additives appear to adversely affect the overall efficiency.

To qualitatively examine the effect of the confined environment of the gear pump on the graphite, ESEM images of the additives were taken before and after the experiments. Figures 14a and 14b show images of graphite flakes before (a) and after (b) running through the gear pump. The lamellar structure which makes graphite a well-documented lubricant can be seen in Figure 14a. As seen in Figure 14b, the same lamellar structure appears to have been well persevered after running through the pump suggesting that graphite was not degraded during the experiment.

### **3.2 Pump Two**

In order to better understand and build upon the promising results obtained from the graphite-ethanol suspensions, multi-walled carbon nanotubes from Sigma Aldrich (described in Table 2 found in Section 5 of Chapter 2) were the next solid additive used to create colloidal suspensions with ethanol. The CNTs and silyl-terminated polyether were added to a plastic reservoir filled with a premeasured amount of ethanol. The mixture was then mechanically shaken until good dispersion was obtained. This process was used to create four different

concentrations (1000, 600, 400, and 200 ppm) of the CNT-ethanol colloidal suspensions. The suspensions were always mechanically shaken prior to testing. Also, the system was allowed to run for at least five minutes before any pressure manipulation was performed which further helped to ensure proper mixing and good additive dispersion. The suspensions were tested in order of increasing concentration (i.e. pure ethanol first and the highest concentration last). The pump was turned on with both the internal pressure relief valve and needle valve completely open. The relief valve was left open in order to obtain a wider range of pressures tested. The internal relief valve was then tightened so that the discharge pressure increased in increments of 2-10 psi (it is difficult to obtain precise pressure adjustments using the internal relief valve). Once the internal relief valve was tightened completely, the needle valve was closed in a manner so that the discharge pressure continued to increase in 5-10 psi intervals. At each of these intervals, the inlet pressure, discharge pressure, volumetric flow rate (obtained from the Omega volumetric flow meter for these experiments), and power consumption data was recorded. After an experiment with a particular suspension was completed, the system was drained, flushed numerous times with pure ethanol, and allowed to dry before the next solution was tested.

This data was used to produce Figure 15. Figure 15 shows volumetric flow rate change as a function of differential pressure across the pump for selected CNT colloidal fluids. This data was plotted to explore the dependence of maximum volumetric flow rate at a given  $\Delta p$  on additive concentration. It appears that the first part of the data points contradict those obtained by Bielmeier et al. in Figure 3. However, once again this can be explained by the use of the internal pressure relief valve in initially raising the pressure as discussed in Section 1 of

Chapter 3. As Figure 15 shows, as the additive concentration is increased the volumetric flow rate increases for a given  $\Delta p$ . Though the 400 ppm, 600 ppm, and 1000 ppm CNT concentrations of Figure 15 produce similar volumetric flow rates for a given  $\Delta p$ , they still produce increases in flow rate over the 200 ppm CNT concentration and pure ethanol. These results again suggest a reduction in internal pump leakage.

To qualitatively examine the effect of the confined environment of the gear pump on the CNTs, ESEM images of the additives were taken before and after the experiments. Figures 16a and 16b show images of CNTs before (a) and after (b) running through the gear pump. Figure 16a shows that they have an average length of around 5-6 micrometers. The CNTs also have an average length of around 5-6 microns in Figure 16b. This indicates that the CNTs were not crushed or broken into smaller pieces by the gear teeth and pump housing. The clumped round residue that can be seen in the images is the cured surfactant (silyl-terminated polyether) that was used to functionalize the surface of the CNTs while they were in suspension to prevent agglomeration.

Since both the graphite-ethanol and CNT-ethanol suspensions had shown to have a positive impact on pump performance, it was necessary to determine the feasibility of their use in a hydraulic system which contained filters. As described in Section 4 of Chapter 2, the first filter to be examined was made of a high consistency polypropylene and had a nominal rating of 30  $\mu\text{m}$ . The filter and its housing were installed in the hydraulic loop in place of the volumetric flow meter shown in Figure 4. The 1550 ppm graphite-ethanol suspension was mechanically mixed, placed in the reservoir, and the system was allowed to run for one hour. The filter was then removed from its housing and can be seen in Figure 17a. The system was

flushed with pure ethanol and a new filter was installed into the housing. The 1000 ppm CNT-ethanol suspension was then mechanically mixed, placed in the reservoir, and the system was allowed to run for one hour. The filter was then removed from its housing and can be seen in Figure 17b. Figure 17 shows that both graphite and CNTs appear to have been caught in their respective filters but the darker color of the filter in Figure 17b suggests that the CNTs were more susceptible to filterability than the graphite flakes. To further examine this, pieces of each filter were removed using scissors and imaged under an ESEM. These images can be seen in Figure 18. Figure 18a once again shows the lamellar structure of the graphite as it appears to coat the polypropylene filter. Figure 18b shows that the CNTs appear to be trapped in between the individual fibers of the filter in large clumps. This makes sense because the CNTs have a strong affinity for one another, and it was more difficult to create stable CNT-ethanol suspensions than graphite-ethanol suspensions. Figure 18 confirms what Figure 17 suggested in that the CNT-ethanol suspensions are more susceptible to filtering than the graphite-ethanol suspensions.

In order to examine how the size and composition of the filter affected the amount of CNT additive that was filtered a mesh screen filter comprised of Type 304 stainless steel and housed in a bronze y-strainer (described in Section 4 of Chapter 2) was tested. The filter and its housing were installed in the hydraulic loop in place of the volumetric flow meter shown in Figure 4. A separate batch of 1000 ppm CNT-ethanol suspension was then mechanically mixed, placed in the reservoir, and the system was allowed to run for one hour. The filter was then removed from its housing and can be seen in Figure 19. In Figure 19a the filter appears darker than in Figure 7, which suggests that CNTs were again filtered out of the suspension. This can

be seen more clearly in Figure 19b in which the mesh screen was cut open and laid flat. This screen was imaged under an ESEM, and Figure 20 shows one of these images. Once again it appears that the CNTs group into large clumps, this time in between the wire meshes. These qualitative observations suggest that filterability is a major issue that needs to be addressed if these suspensions are to be used in an industrial application. One possible solution would be to inject the fluid with more of the additive after every filter location.

### **3.3 Pump Three**

The next nanoadditives to be examined were highly graphitic, Pyrograf-III, carbon nanofibers from Applied Sciences Inc. (described in Chapter 2 Section 2). As previously described the CNFs and SDS were added to a premeasured amount of ethanol, mechanically mixed, and then sonicated to produce the four concentrations (1600, 800, 400, and 200 ppm) of CNF-ethanol suspensions to be tested. The suspensions were always mechanically shaken and sonicated for at least one hour prior to testing. Also, the system was allowed to run for at least five minutes before any pressure manipulation was performed which further helped to ensure proper mixing and good additive dispersion. The suspensions were tested in order of increasing concentration (i.e. pure ethanol first and the highest concentration last). The pump was turned on with the internal pressure relief valve completely closed and the needle valve completely open. The needle valve was then closed in a manner so that the discharge pressure increased in intervals of approximately 5 psi. At each of these intervals, the inlet pressure, discharge pressure, volumetric flow rate (obtained from the Assured Automation volumetric flow meter for these experiments), and power consumption data was recorded. After an

experiment with a particular solution was completed, the system was drained, flushed numerous times with pure ethanol, and allowed to dry before the next solution was tested.

This data was used to produce Figures 21-23. To assess the additive performance on mechanical efficiency, the power consumption of the pump was recorded as a function of differential pressure across the pump. The results for pure ethanol and for the CNF colloidal suspensions can be seen in Figure 21. The results indicate a linear increase in power as the differential pressure across the pump increases, consistent with theoretical trends. Note that for a given pressure drop across the pump, no change in pump power consumption was observed as a function of CNF concentration compared to pure ethanol. In other words, the power required at a given  $\Delta p$  is essentially independent of additive concentration. Therefore, changes in mechanical efficiency due to possible hydraulic fluid viscosity changes can once again be ruled out. Figure 22 shows volumetric flow rate change as a function of differential pressure across the pump for selected CNT colloidal fluids. This data was plotted to explore the dependence of maximum volumetric flow rate at a given  $\Delta p$  on additive concentration. The maximum flow line and mineral oil data points have been added for reference to further exemplify the effects of viscosity and increasing pressure on the volumetric flow rate of the pump. Since the internal relief valve was not used for pressure manipulation in these experiments, Figure 22 follows the trend shown in Figure 3. As Figure 22 shows, as the CNF additive concentration is increased the volumetric flow rate increases for a given  $\Delta p$ . This effect is particularly pronounced at higher pressures, and it can be seen that the higher concentrations of CNFs move the volumetric flow rate towards that of mineral oil. In other words, the CNF additives appear to give the ethanol the volumetric benefit of a higher viscosity

fluid without sacrificing mechanical efficiency. Possible mechanisms for this effect are discussed in Section 1 of Chapter 4. Figure 23 shows overall efficiency as a function of differential pressure across the pump for the different CNF suspensions and pure ethanol. Once again, the overall efficiency was calculated as the power output by the pump divided by the power input to the pump by the motor. It can be seen that the higher concentrations of additives improve the overall efficiency of the pump especially at higher pressures. A number of experiments were conducted to find out whether the closed loop hydraulic system had pressure dependent hysteresis. This was investigated by slowly lowering the pressure differential once the maximum  $\Delta p$  was reached (backward loop) and measuring volumetric flow rate and power. The data points for the 800 ppm overall efficiencies for the forward and backwards loops in Figure 23 are nearly identical which demonstrate that the results are essentially independent of whether pressure is moved from low to high or high to low. In other words, little hysteresis exists between forward and backward loops in this experiment.

To qualitatively examine the effect of the confined environment of the gear pump on the CNFs, ESEM images of the additives were taken before and after the experiments. The CNFs were observed to undergo probable scission after running through the pump. Figure 24a shows the micro-structure of highly entangled and bundled as-received CNF powder. After sonicating in ethanol with the help of a surfactant to form the colloidal CNF suspensions, CNFs appear to disentangle and show a good degree of dispersion as shown in Figure 24b. From Figures 24a and 24b, it can be seen that the pre-run images corresponding to the two different types (as received powder and sonicated) appear similar in structural make-up with the exception of the CNFs in Figure 24b being more dispersed due to sonication. This shows that

sonicating the CNFs in solution does not change their structure. However, the CNFs in Figure 24c look thinner than the CNFs in the pre-run images and also appear to have a film or a shell surrounding them. The film or shell that surrounds the CNFs in this image could possibly be the residual surfactant (SDS) coating on the graphitic surfaces of the CNFs. The CNFs also appear shorter in length in Figure 24c than in Figures 24a and 24b. This suggests that possible scission of the CNFs is occurring within the gear pump in time. However, it is still unclear whether the structural changes in CNFs during pump operation has a direct effect on the pump efficiency in the long run. During the pump operation times of this study (~30 min), the structural changes in CNFs do not seem to reduce the increase in pump efficiencies.

### **3.4 Pump Four**

The final nanoadditives to be tested were the two different aspect ratio multi-walled CNTs from Nanoamor (described in Table 2 found in Section 5 of Chapter 2). As previously described the CNTs and SDS were added to a premeasured amount of ethanol, mechanically mixed, and then sonicated to produce the two concentrations (1000 and 500 ppm) of CNT-ethanol suspensions to be tested. The suspensions were always mechanically shaken and sonicated for at least one hour prior to testing. Also, the system was allowed to run for at least five minutes before any pressure manipulation was performed which further helped to ensure proper mixing and good additive dispersion. The suspensions were tested in order of increasing concentration (i.e. pure ethanol first and the highest concentration last). The pump was turned on with the internal pressure relief valve completely closed and the needle valve completely open. The needle valve was then closed in a manner so that the discharge pressure increased in intervals of approximately 5 psi. At each of these intervals, the inlet pressure, discharge

pressure, volumetric flow rate (obtained from the Assured Automation volumetric flow meter for these experiments), and power consumption data was recorded. After an experiment with a particular solution was completed, the system was drained, flushed numerous times with pure ethanol, and allowed to dry before the next solution was tested.

The data from the CNT suspensions with an aspect ratio of 10-25 was used to produce Figures 25-27 while the data from the CNT suspensions with an aspect ratio of 200-250 was used to produce Figures 28-30. Figure 25 and Figure 28 show the power consumption of the pump as a function of differential pressure across the pump for their respective CNT suspensions. Both these figures show that the CNT-ethanol suspensions increase the power required over that of pure ethanol for a given differential pressure. Figure 26 and Figure 29 show the volumetric flow rate as a function of differential pressure across the pump for their respective CNT suspensions. Both these figures show that the CNT-ethanol suspensions decrease the flow rate produced compared to that of pure ethanol for a given differential pressure. Figure 27 and Figure 30 show the overall efficiency as a function of differential pressure across the pump for their respective CNT suspensions. Both these figures show that the CNT-ethanol suspensions decrease the overall efficiency obtained compared to that of pure ethanol for a given differential pressure. All these results suggest that the CNT-ethanol suspensions are adversely affecting the pump performance, and these adverse effects are more pronounced for the 1000 ppm suspensions than the 500 ppm suspensions. This is in direct contrast to the results obtained for the graphite, CNTs of aspect ratio 45-53, and CNFs tested in different pumps. A possible reason why this may have occurred is discussed in Section 1 of Chapter 4.

### 3.5 Discussion

The results of this study suggest that the use of graphite, carbon nanotubes, and carbon nanofibers as solid additives in ethanol colloidal suspensions may reduce internal leakage in an external gear pump. It can be difficult to explain this effect because film thickness variations between gear teeth indicate a complex tribological condition due to variable sliding speed and strong variation in pressure and radius of curvature [15]. Graphite, CNT, and CNF additives in the hydraulic fluid are all forced to confine themselves in these small complex clearances in an unsteady fashion. Furthermore, Wedeven and Bourdoulous [16] note that asperity stress, particularly during initial pump operation, can gear pump internal leakage. The area of most concern in the gear pumps with respect to lubrication is the region of high sliding near the root and tip of the gear teeth [16]. These are the regions where insufficient elastohydrodynamic film thickness is present. In general, good film forming hydraulic fluids can partially alleviate the resulting problems such as local adhesion, wear and scuffing. In addition, there have been some improvements in the design of gears from materials with smoother surface finishes [17].

When graphite surfaces with very small amounts of surface-adsorbed liquids slide against metal surfaces, the amount of metal debris loss from the surfaces (wear) was shown to be reduced drastically [18]. This can be attributed to local increases in additive concentration in the small clearance regions. At such graphite concentrations, graphite-metal contacts are expected to be established between the additive and the gear tooth surface which help reduce wear. As such, the present graphite, CNT, and CNF additives may fill the asperities (caused by machining or wear on the gear surfaces) thus reducing the available leak paths, i.e. effectively smoothing the surfaces locally. This hypothesis is consistent with observations by Lu et. al. [19]

whereby dispersed carbon nanotube (CNT)/polymer mini-emulsions (suspensions) were found to fill micro-gaps of the rubbing surfaces as long as the CNT concentrations were kept below 2000 ppm. Thus, the present additives may reduce leakage by reducing the effective clearance through a reduced effective roughness. It should be noted that when pure ethanol was run through the pump after the colloidal suspensions, increased flow rates were still sustained for some time. This further supports the possibility that the additives may adhere to the asperities of the metal surfaces.

It is important to note that the reduction in effective clearance does not lead to an increase in power consumption which can accompany low viscosity fluids (Figures 11 and 21). This suggests that a second mechanism associated with improved lubrication is also important to explain the overall behavior. The results of Lu et. al. [19] showed that the suspensions were found to form a self-assembled lubricating thin film, creating a roller-bearing effect. It can be hypothesized that the graphite, CNT, and CNF particles also allow such a roller bearing effect as shown in Figure 31. In particular, it can be expected that they form thin permanent lubricating layers penetrating into the surface asperities on gear surfaces as the surfaces mate during pump operation.

However, the effectiveness of the roller-bearing effect may depend on the chemical and geometric features of the additives as well as the concentration and the degree of colloidal dispersion in the solutions [19]. Such differences are manifested in Figures 12, 15, and 22, whereby the increases in flow rate are not linearly related to concentration and the way in which they behave differs. At high concentrations, graphite and CNT suspensions have little leakage such that the flow rate is near the maximum value over a wider range of pressures than

seen for pure ethanol. However, the flow rate drops off rapidly when the differential pressure reaches and exceeds 500 kPa as seen in Figures 12 and 15. In the case of CNF additives, the increase in flow rate over pure ethanol becomes more pronounced as pressure rise moves to higher values. This suggests that graphite and CNT may be more beneficial as additives at lower pressures and CNFs may be more effective at higher pressures. Perhaps, one may design novel low-viscosity hydraulic fluids with a combination of conventional and nanoscale colloidal additives for efficient pump operation over a range of pressures.

The CNTs used in pump four, however, adversely affected the pump performance. This may be explained with the aid of Figure 32 which shows the volumetric flow rate of ethanol as a function of differential pump pressure for each of the four pumps used for these experiments. Though all pumps were the same model and all came from the same manufacturer, it is virtually impossible to make every single part of every pump identical especially at the nanoscale level. This is further suggested by Figure 32. By looking at Figure 32, it can be seen that pumps one, two, and three all had a maximum flow rate of approximately 4.5 to 4.9 liters/min. However, pump four had a maximum flow rate of approximately 5.8 liters/min. This suggests that the parts of every pump can have slightly different geometrical constructions which caused them to have different levels of internal leakage. These constructions are also extremely sensitive to any change in their assembly. For example, after testing with pump one was completed, the pump was disassembled for examination. It was then reassembled and when ethanol was run through it again there was a large reduction in flow rate and high amount of cavitation in the line. Figure 32 suggests that pump four had the least amount of internal leakage. It can be hypothesized that pump four may have had the minimum amount of

internal leakage obtainable for this particular pump design. By introducing the CNTs into this pump, they were effectively increasing the gaps through which internal leakage occurs and adversely affecting the pump performance.

### 3.6 Figures

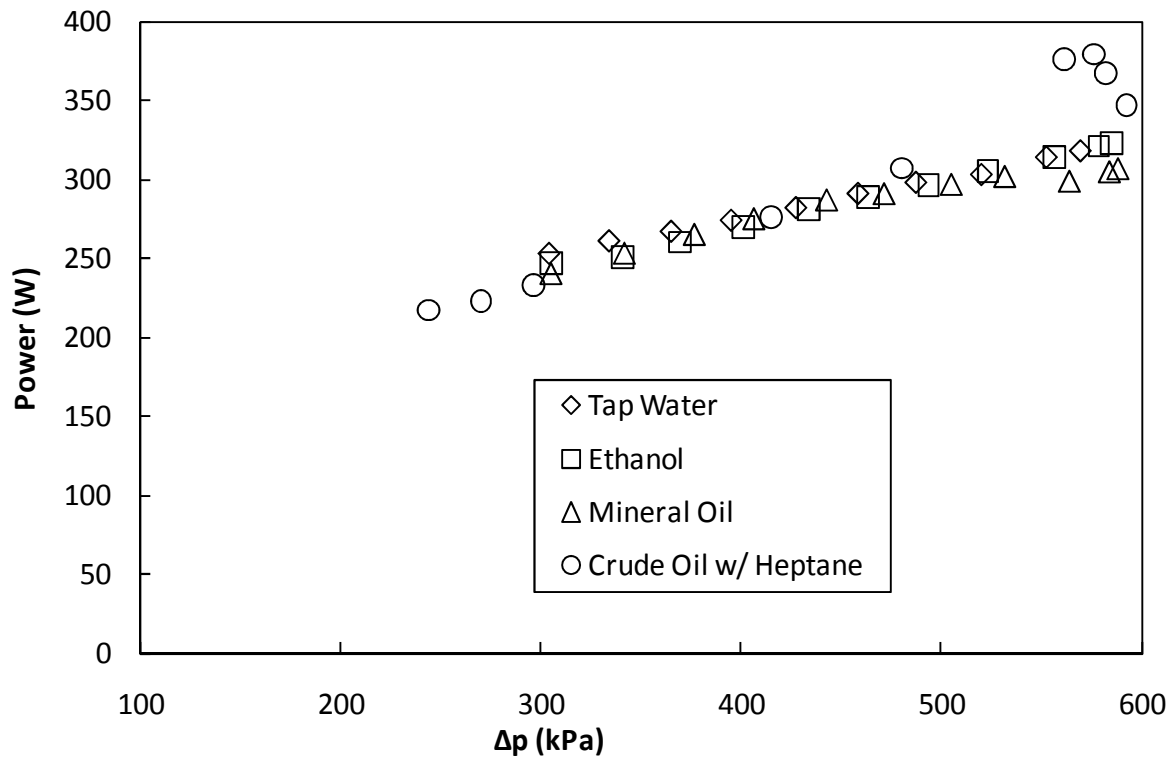


Figure 8. Pump power required as a function of differential pump pressure for four different fluids.

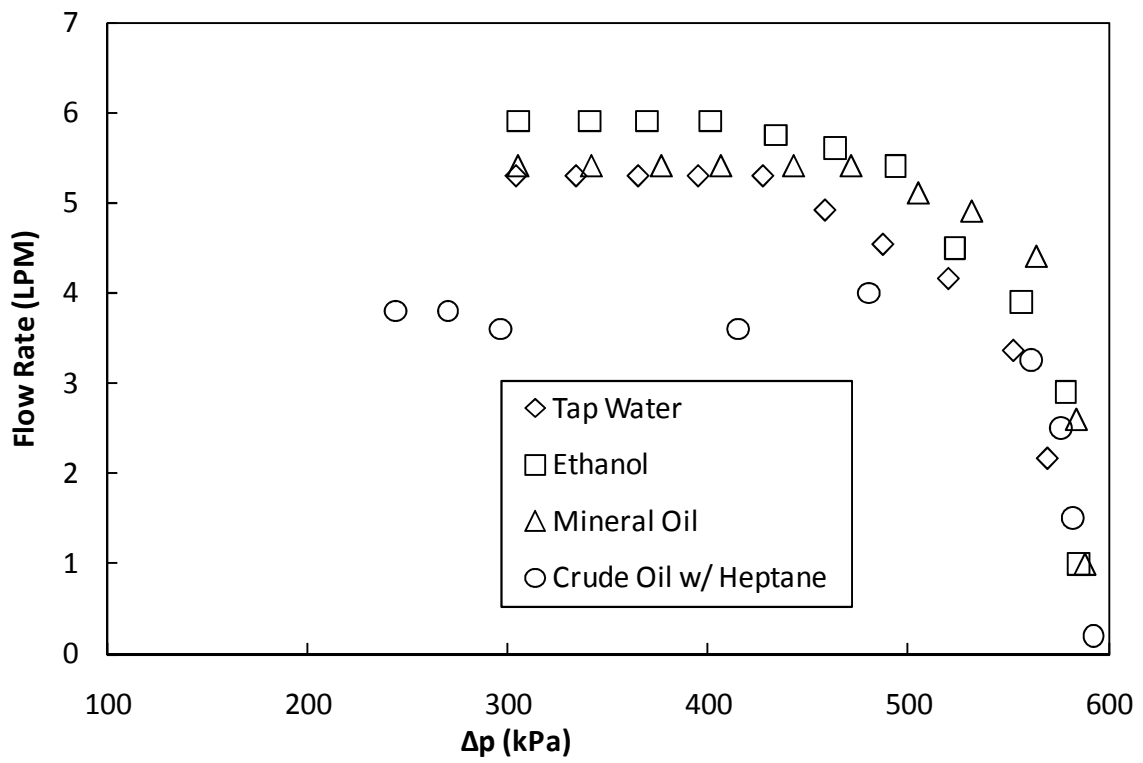


Figure 9. Volumetric flow rate as a function of differential pump pressure for four different fluids.

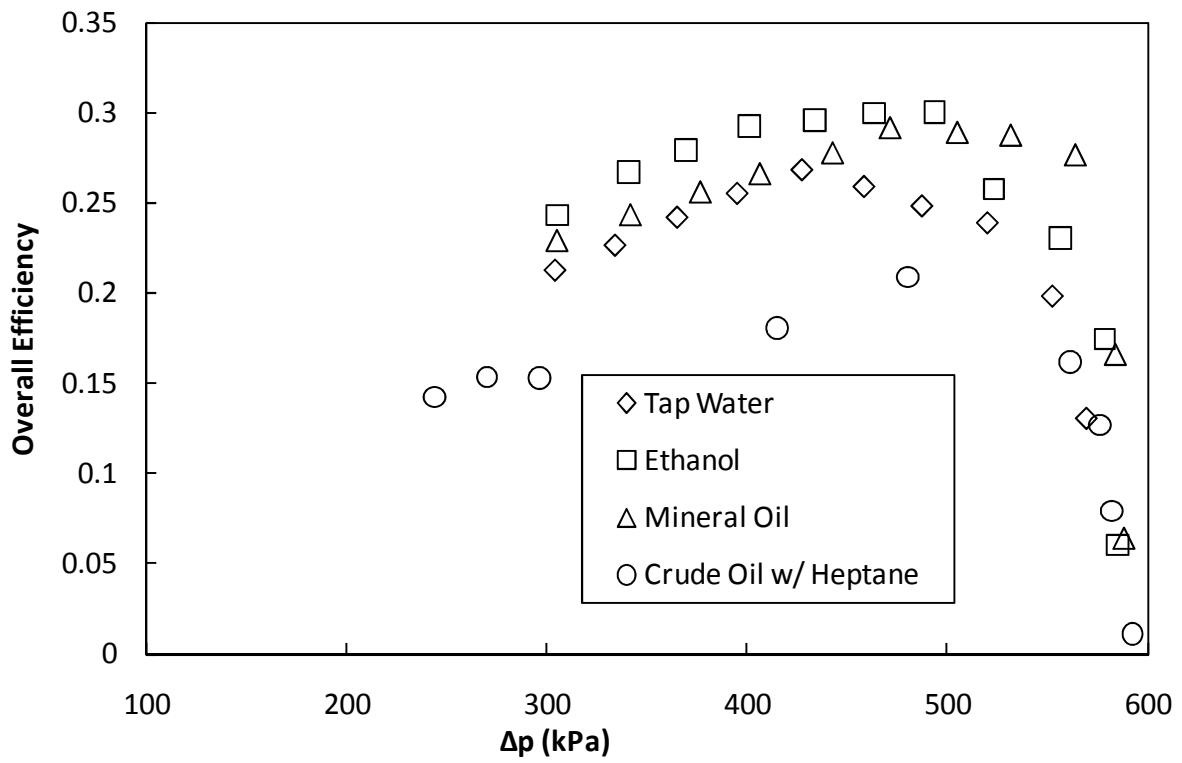


Figure 10. Overall efficiency as a function of differential pump pressure for four different fluids.

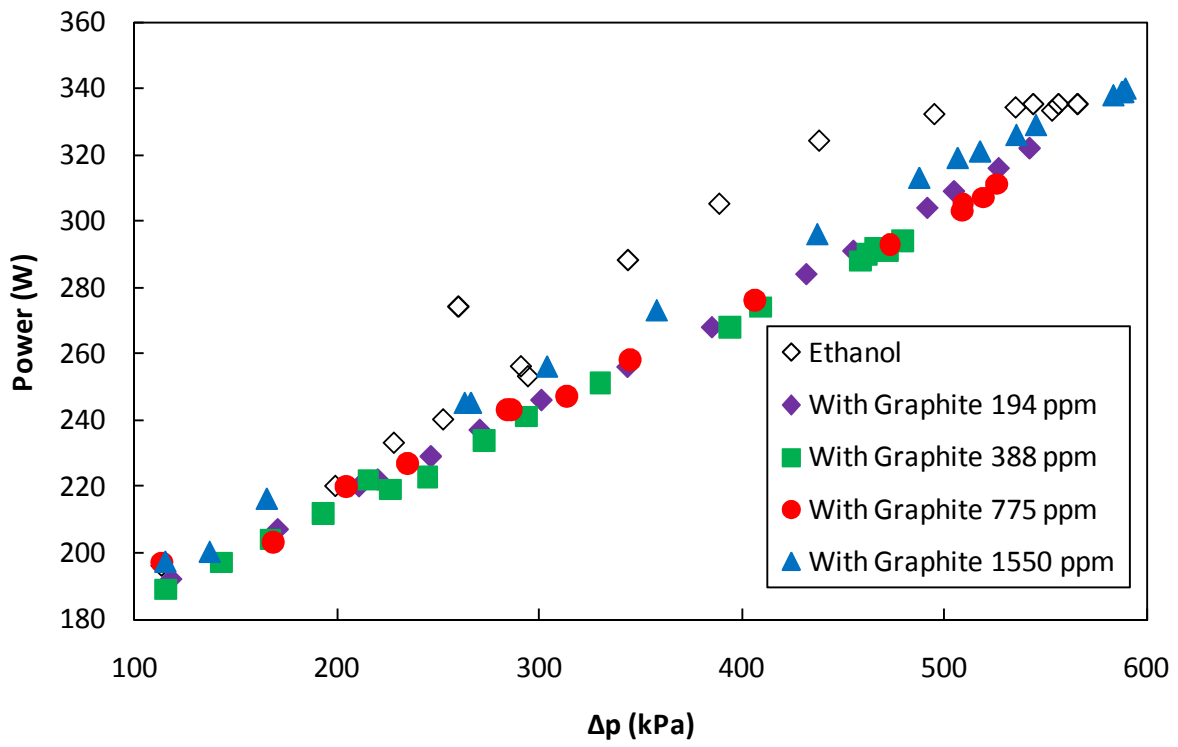


Figure 11. Power as a function of differential pump pressure for graphite suspensions.

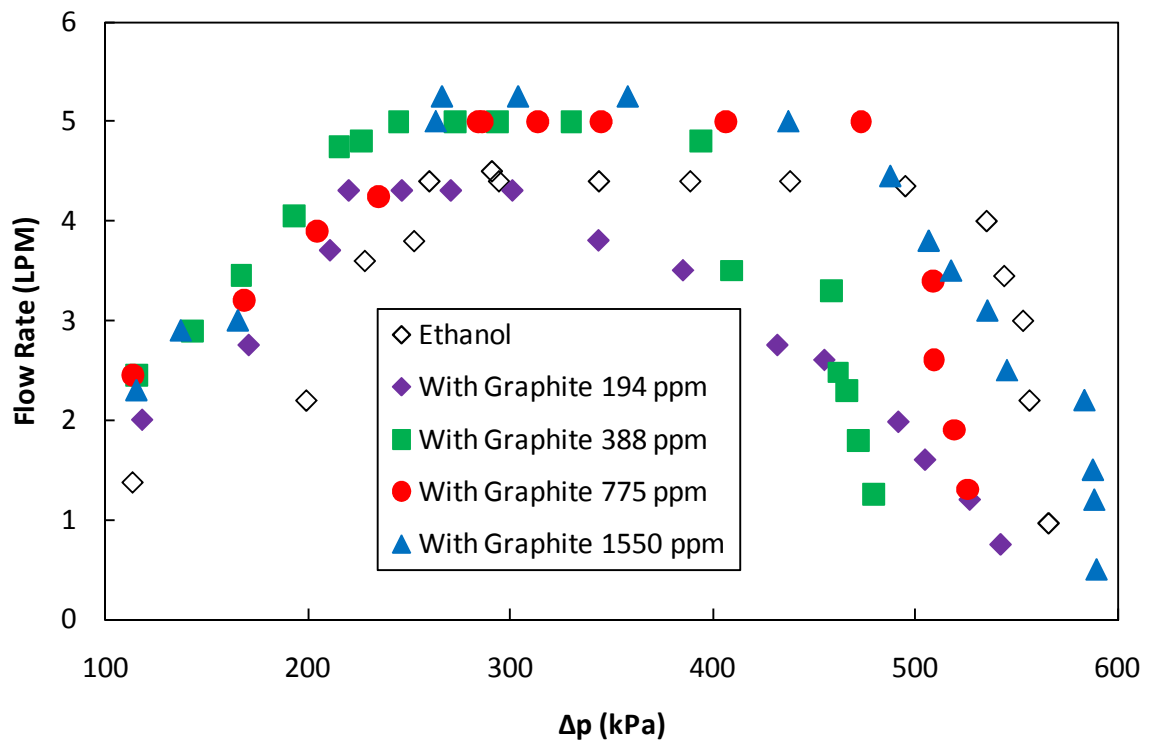


Figure 12. Volumetric flow rate as a function of differential pump pressure for graphite suspensions.

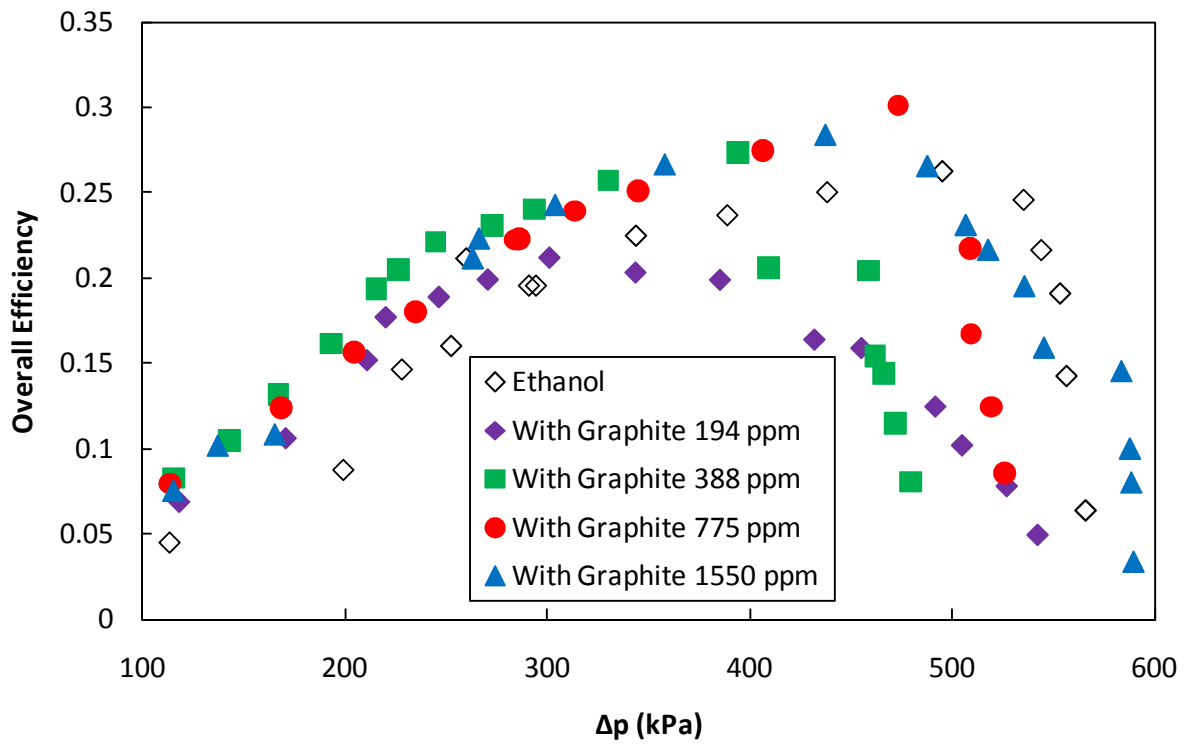
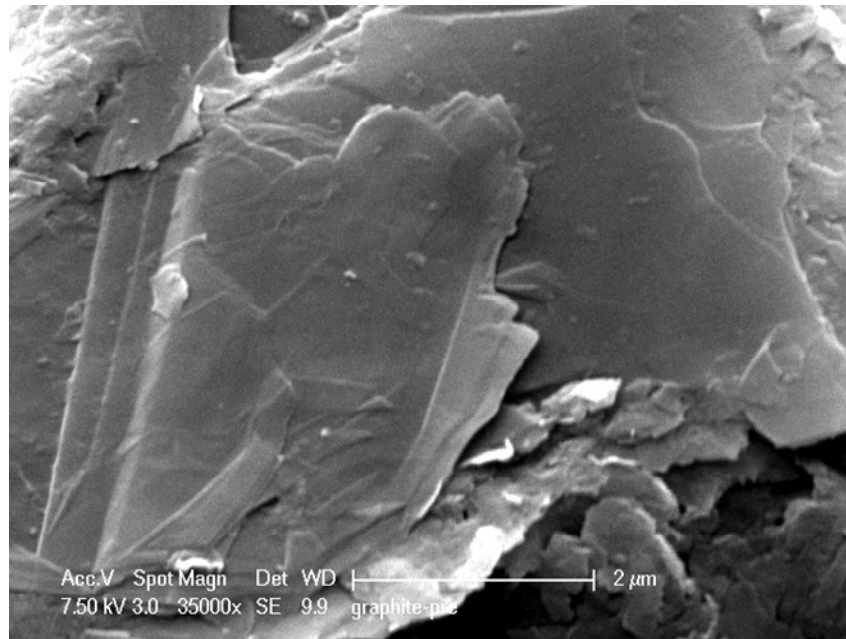


Figure 13. Overall efficiency as a function of differential pump pressure for graphite suspensions.

(a)



(b)

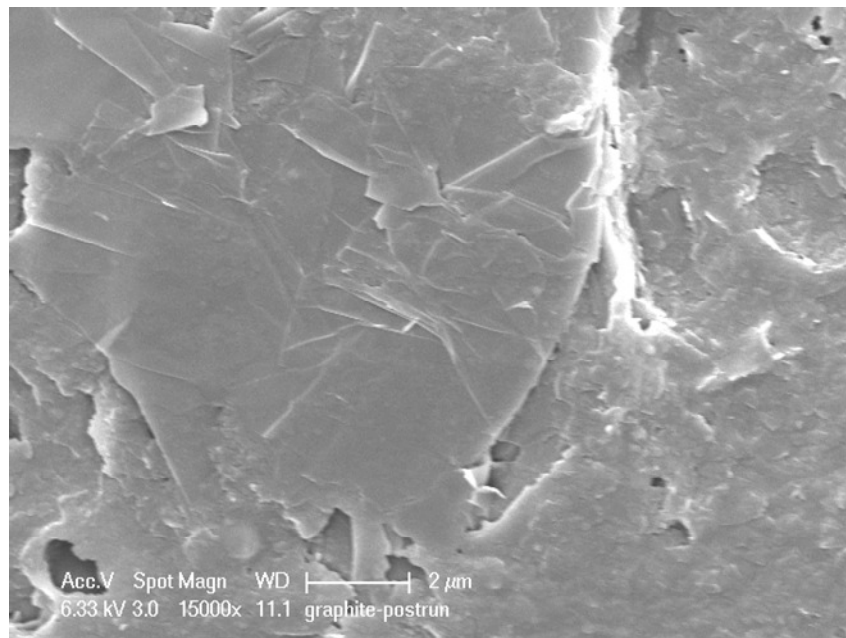


Figure 14. Scanning electron microscope images of graphite (a) as received and (b) post-experiment.

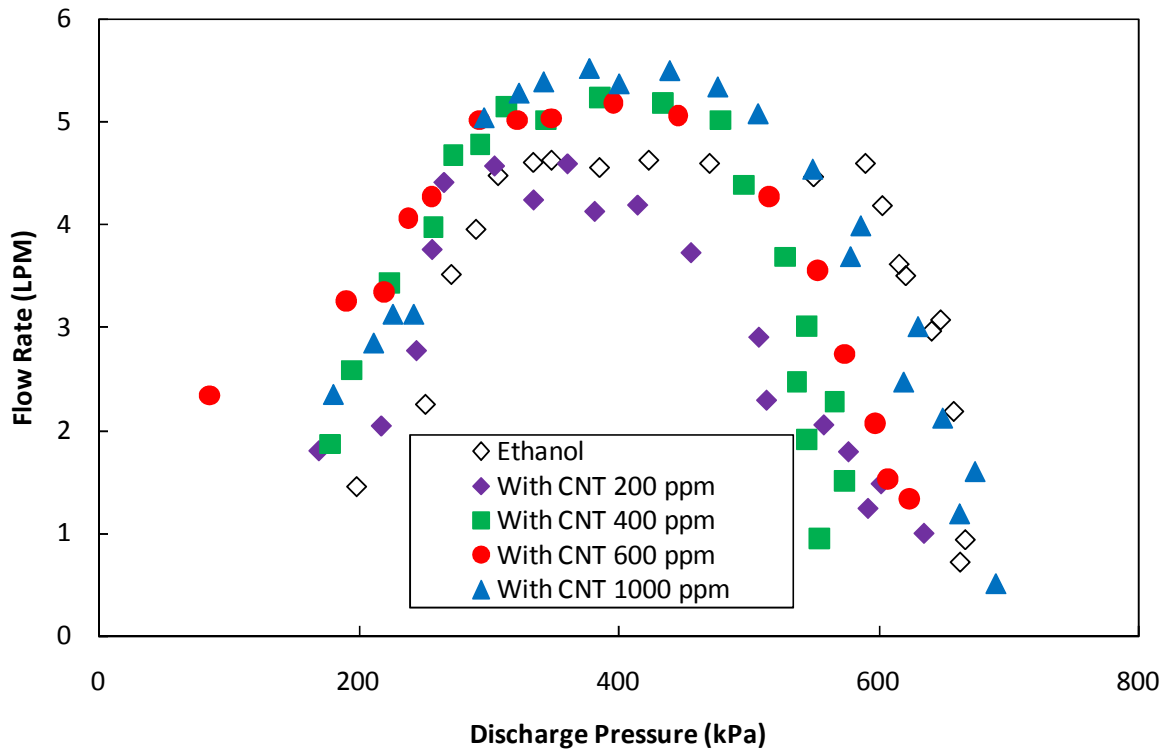
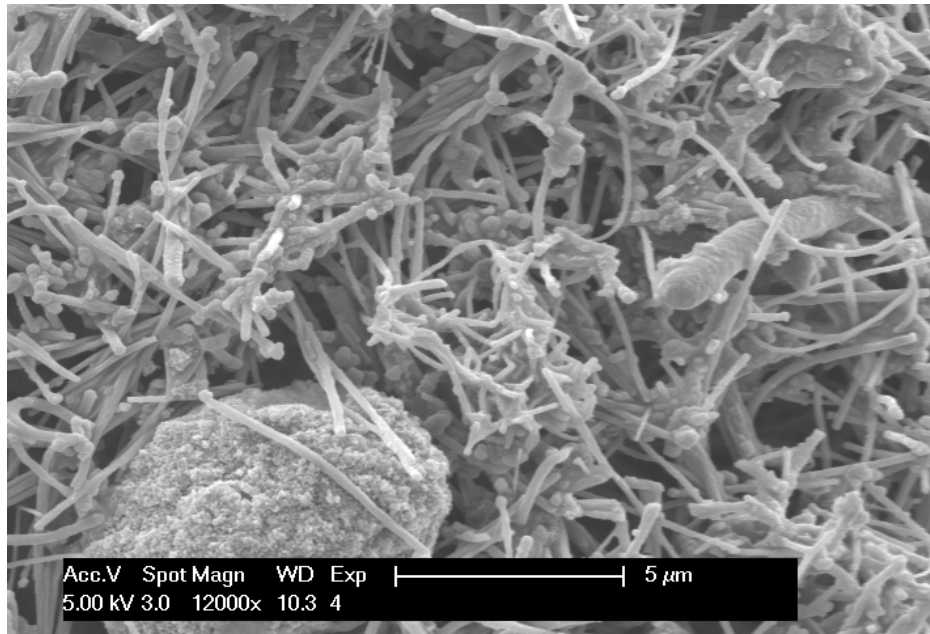


Figure 15. Volumetric flow rate as a function of discharge pressure for CNT (d= 110-170 nm and l= 5-9  $\mu$ m) suspensions.

(a)



(b)

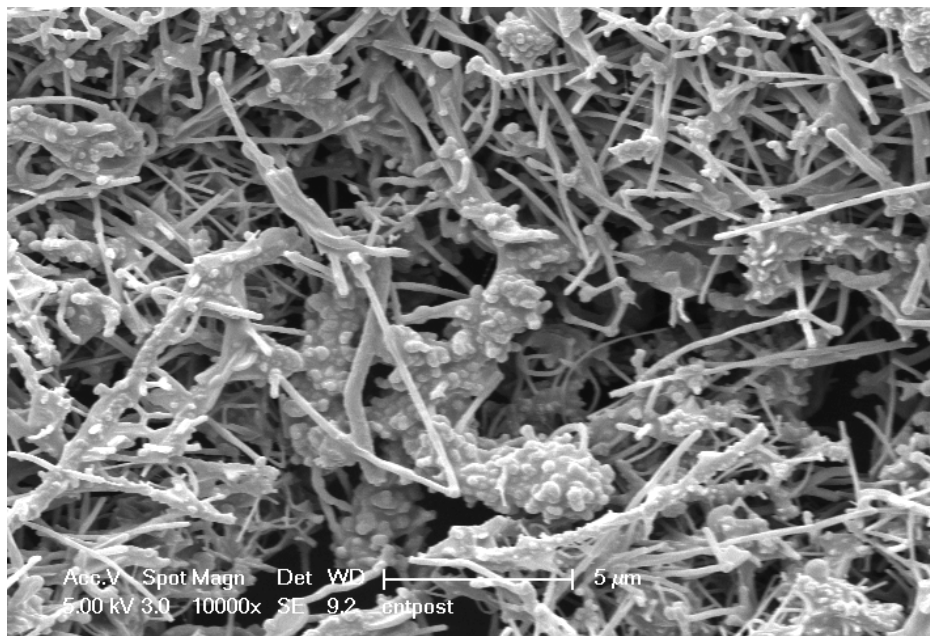


Figure 16. Scanning electron microscope images of CNTs (a) as received and (b) post-experiment.

(a)

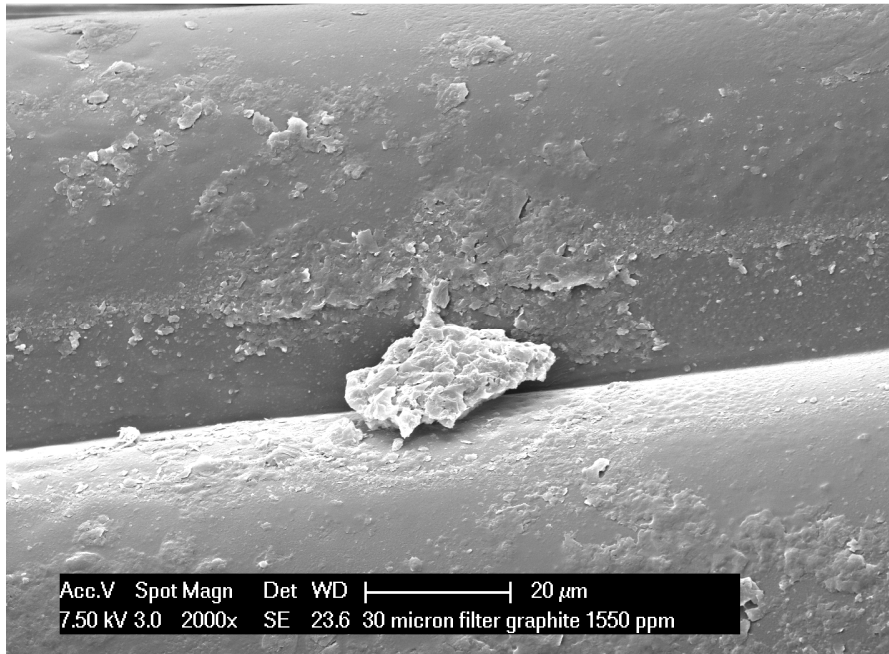


(b)



Figure 17. Claris Series filter from the Pall Corporation (a) after 1550 ppm graphite-ethanol suspension run and (b) after 1000 ppm CNT-ethanol suspension run.

(a)



(b)

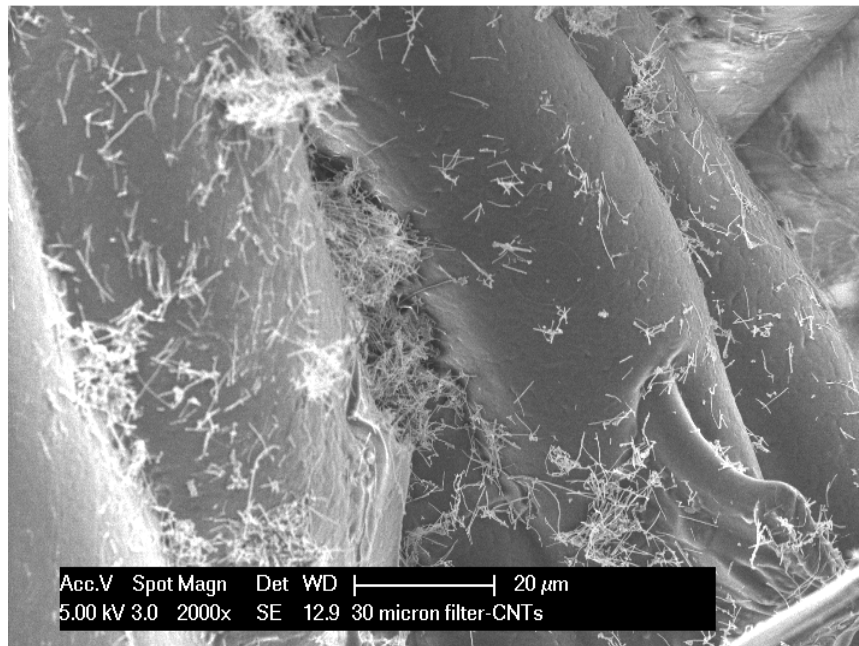


Figure 18. Scanning electron microscope images of Claris Series filter from the Pall Corporation (a) after 1550 ppm graphite-ethanol suspension run and (b) after 1000 ppm CNT-ethanol suspension run.

(a)



(b)



Figure 19. Mesh screen filter from McMaster-Carr after 1000 ppm CNT-ethanol suspension run (a) intact and (b) cut open and laid flat.

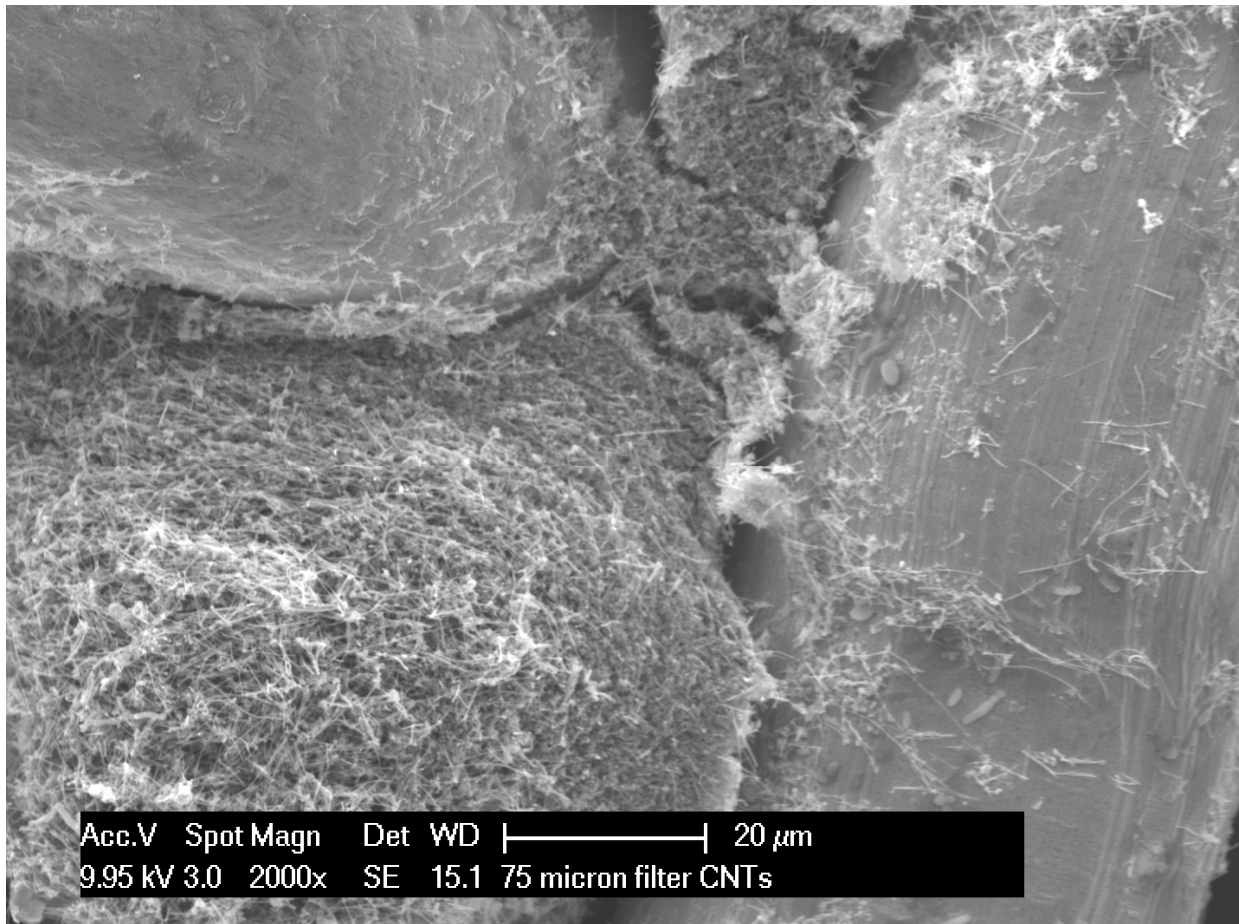


Figure 20. Scanning electron microscope image of Mesh screen filter from McMaster-Carr after 1000 ppm CNT-ethanol suspension run.

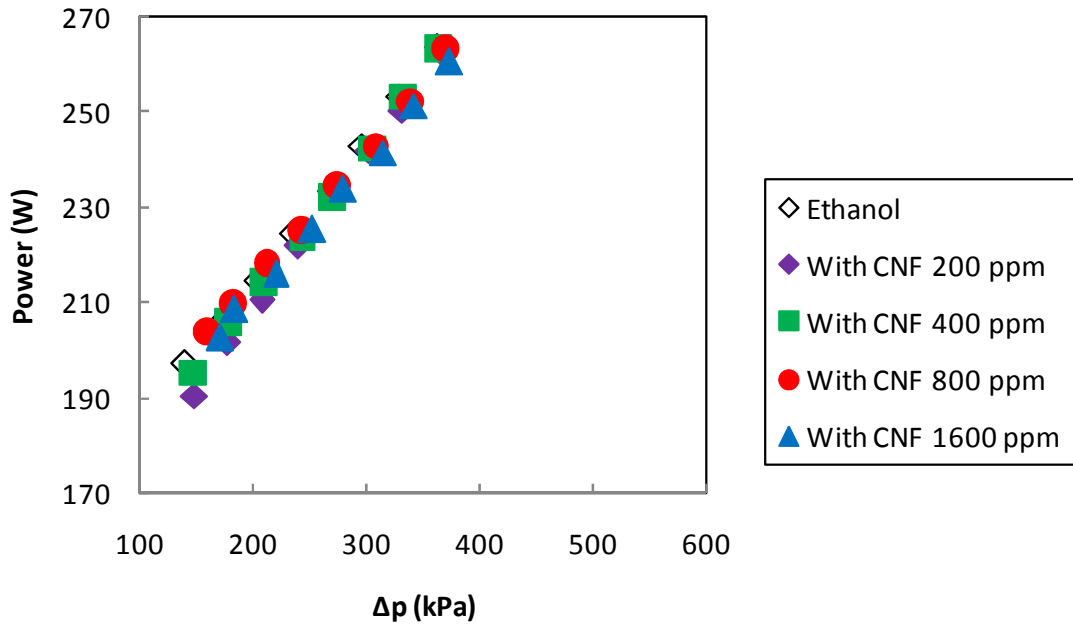


Figure 21. Power as a function of differential pump pressure for CNF suspensions.

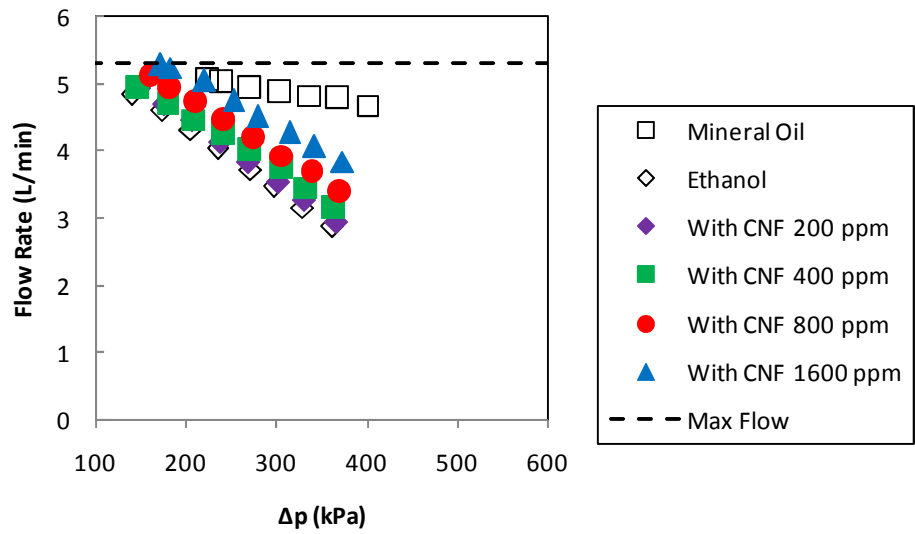


Figure 22. Volumetric flow rate as a function of differential pump pressure for CNF suspensions.

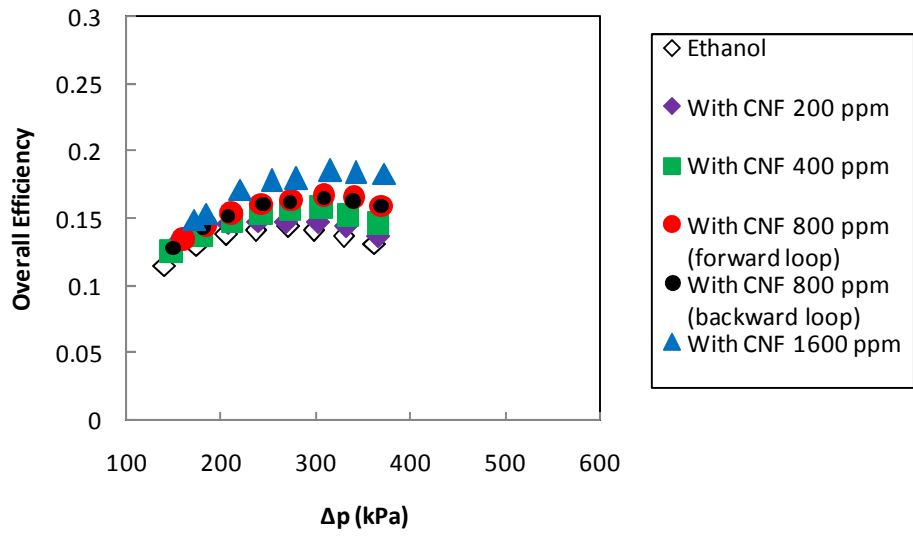


Figure 23. Overall efficiency as a function of differential pump pressure for CNF suspensions.

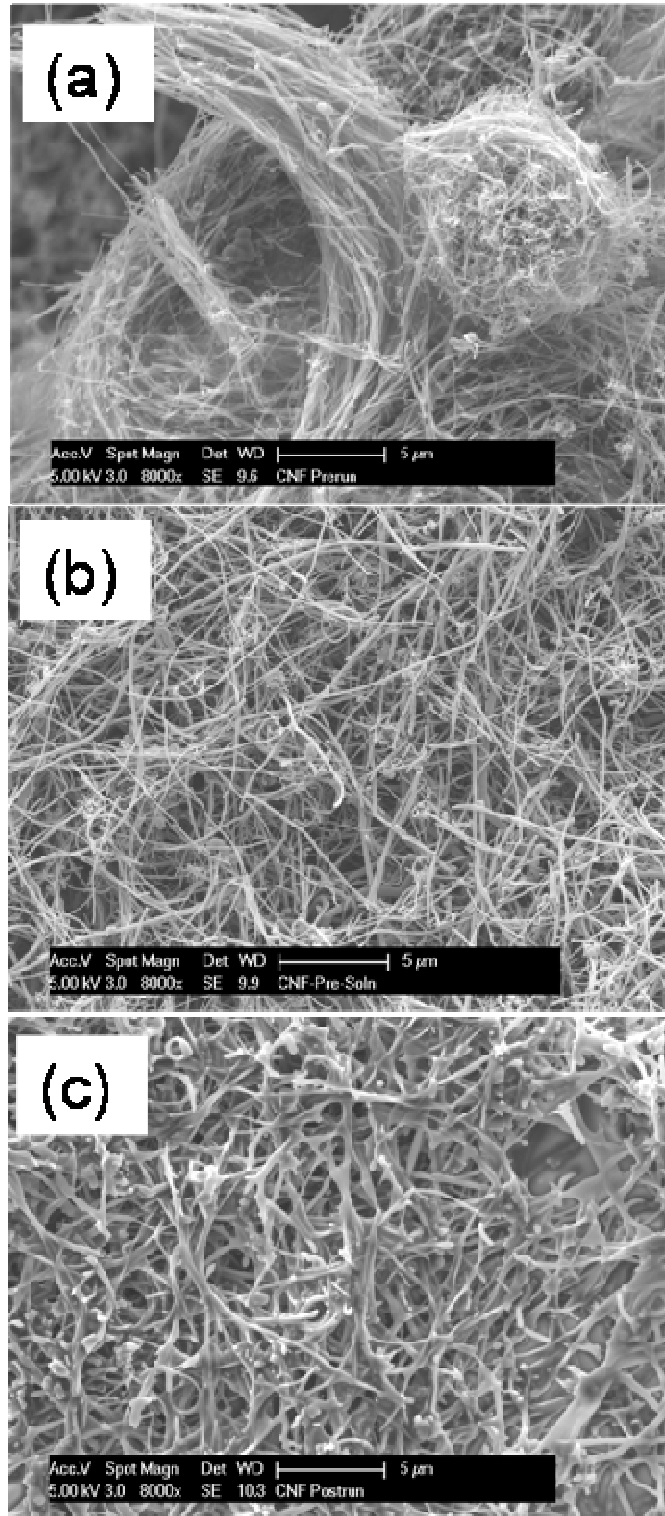


Figure 24. Scanning electron microscope images of CNFs (a) as received, (b) from sonicated solution, and (c) post-experiment.

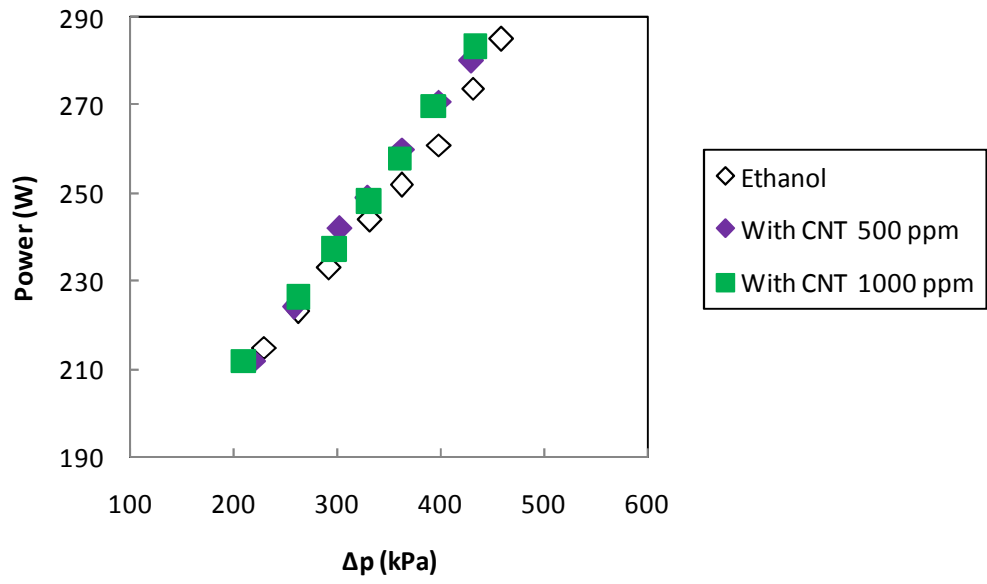


Figure 25. Power as a function of discharge pressure for CNT ( $d= 50-80$  nm and  $l= 0.5-2.0$   $\mu\text{m}$ ) suspensions.

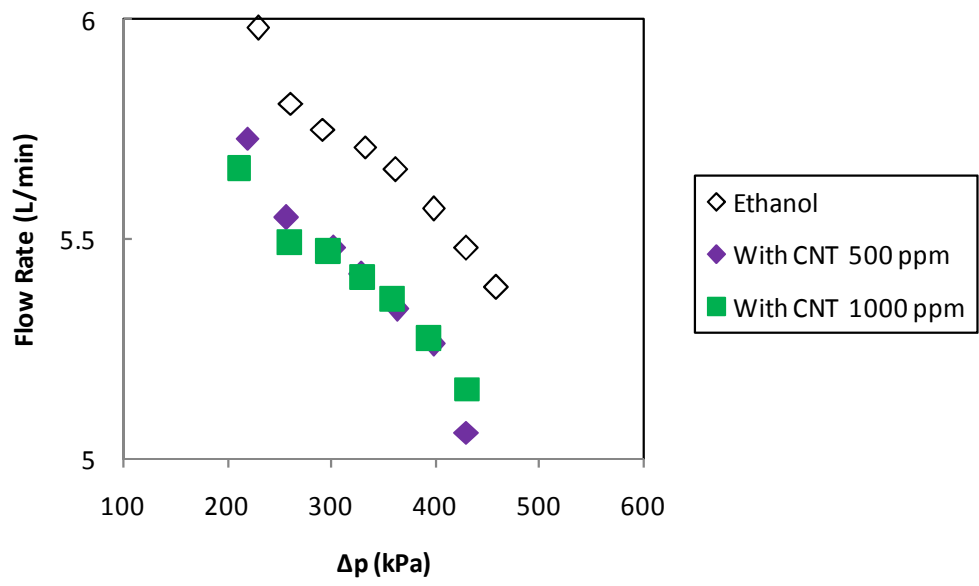


Figure 26. Volumetric flow rate as a function of discharge pressure for CNT (d= 50-80 nm and l= 0.5-2.0 μm) suspensions.

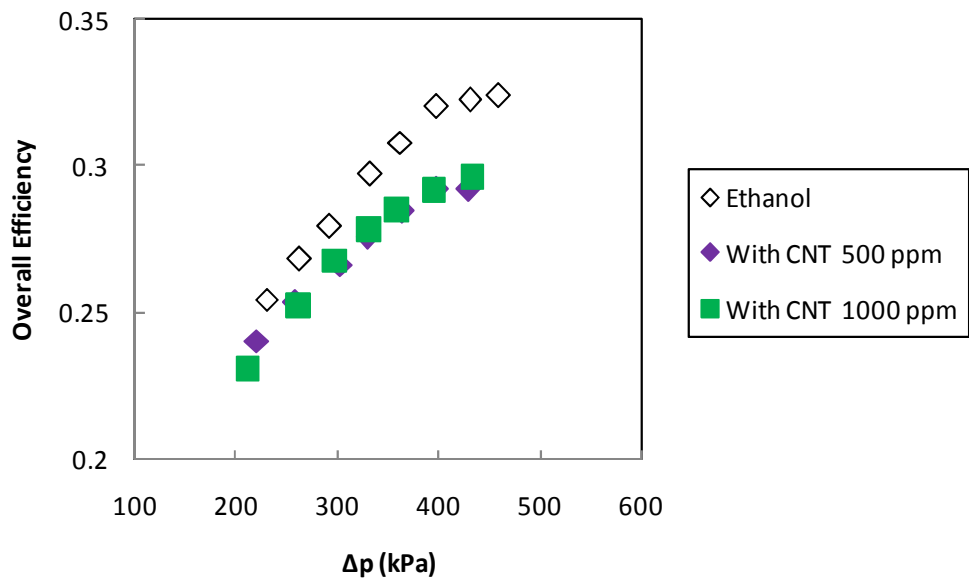


Figure 27. Overall efficiency as a function of discharge pressure for CNT (d= 50-80 nm and l= 0.5-2.0 μm) suspensions.

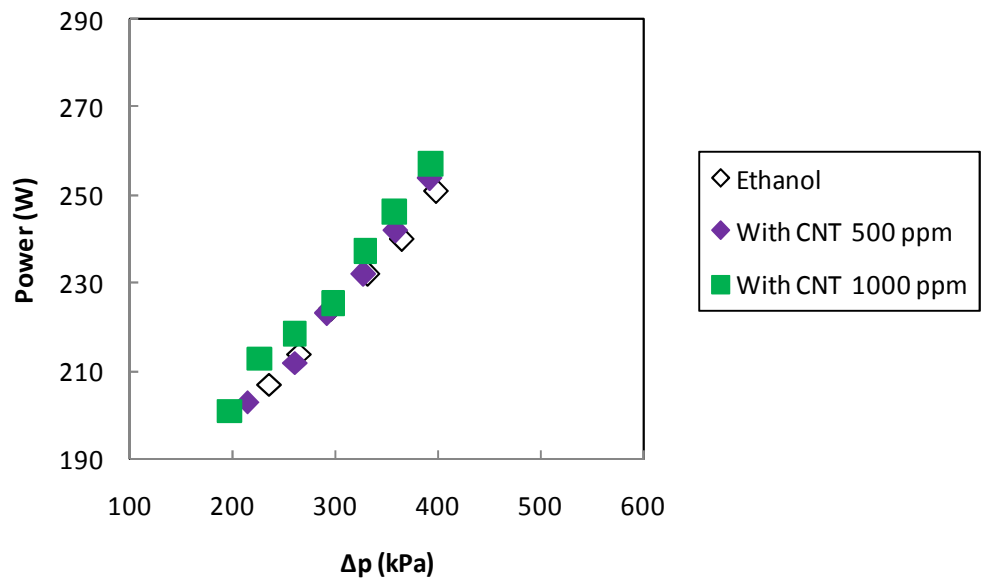


Figure 28. Power as a function of discharge pressure for CNT ( $d= 50-80$  nm and  $l= 10-20$   $\mu\text{m}$ ) suspensions.

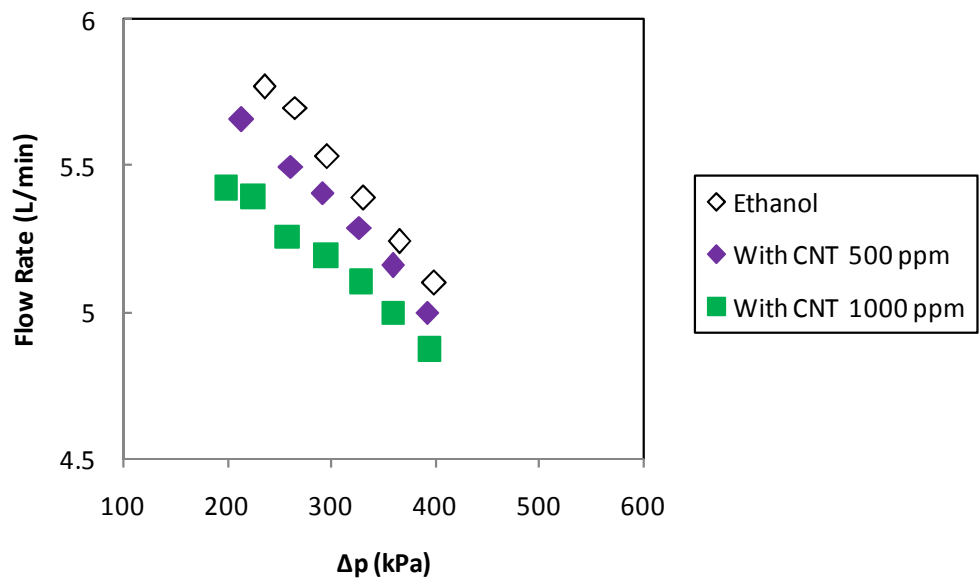


Figure 29. Volumetric flow rate as a function of discharge pressure for CNT ( $d= 50-80$  nm and  $l= 10-20$   $\mu\text{m}$ ) suspensions.

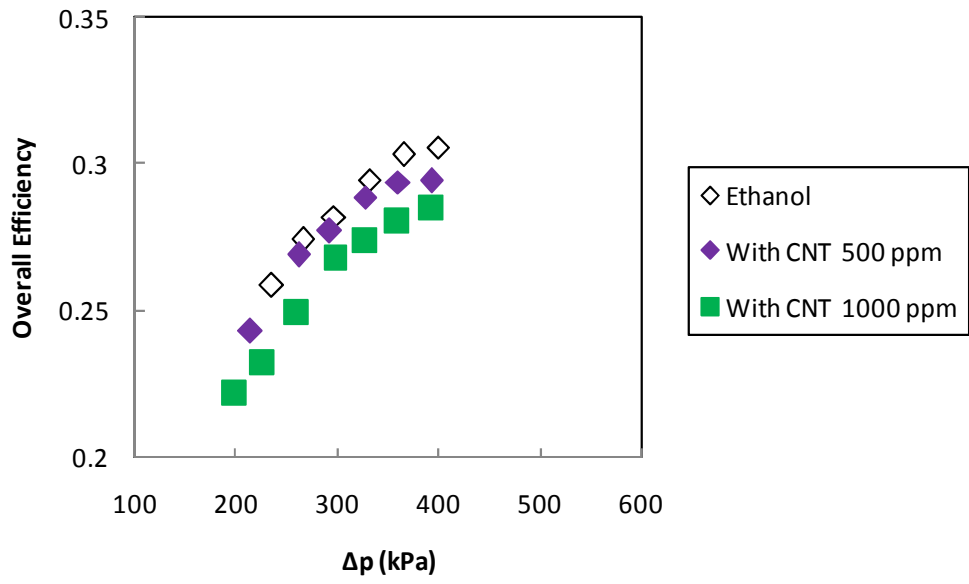


Figure 30. Overall efficiency as a function of discharge pressure for CNT (d= 50-80 nm and l= 10-20 μm) suspensions.

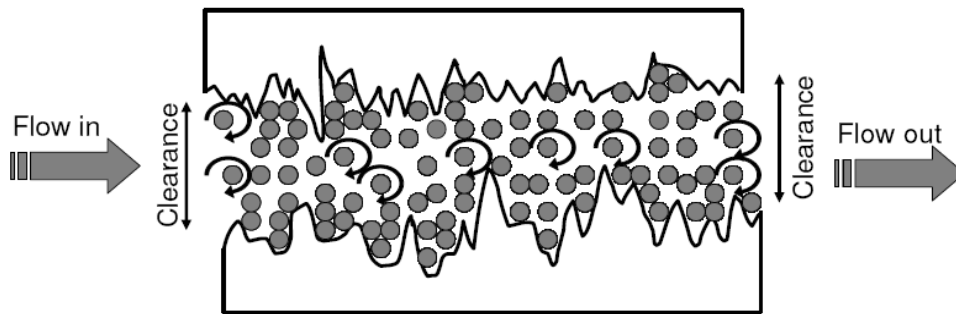


Figure 31. Schematic showing CNF or graphite induced micro roller bearing effect within the clearances formed by engaging gear surfaces during pump operation. The additives also smooth out the asperities on the as-machined gear surfaces by self-assembling into them.

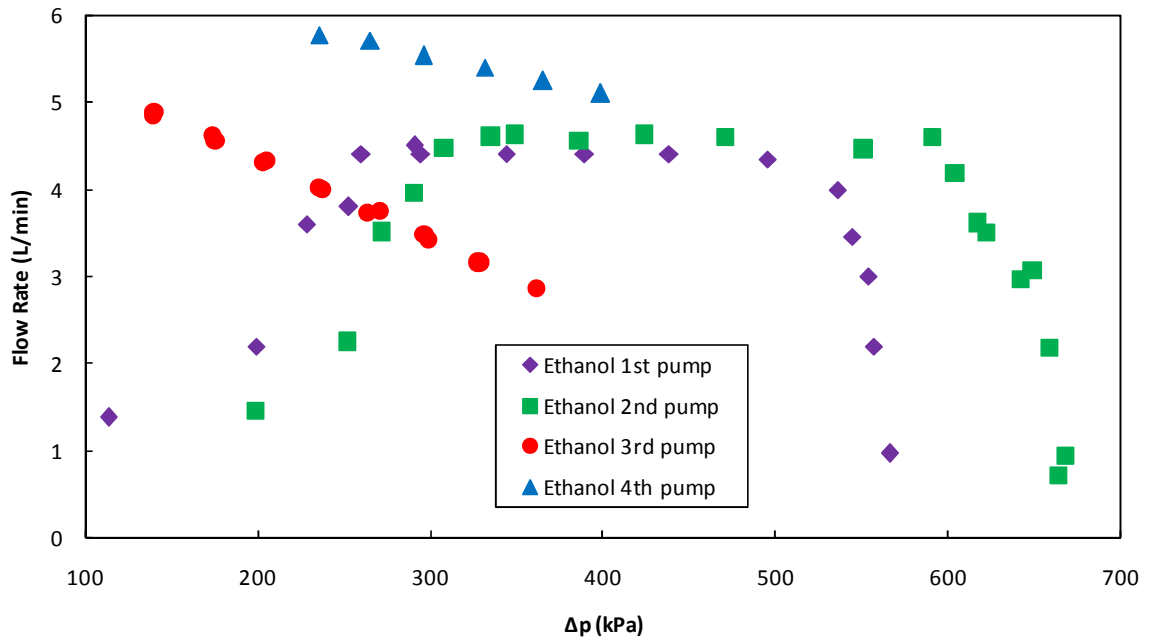


Figure 32. Volumetric flow rate as a function of discharge pressure for pure ethanol for each different pump used in testing.

## Chapter 4: Conclusions

Graphite, CNTs, and CNFs have all shown to positively impact external gear pump performance when used as additives for low viscosity fluids. The ideal concentration range was found to be between 400 to 1600 ppm. To the author's knowledge, this is the first study to show that additives can increase volumetric efficiency without significantly increasing the viscosity of the working fluid (ethanol). Higher concentrations (> 400 ppm) of the additives produced more profound positive effects than the lower concentrations. Also, the power consumption was independent of additive concentration, leading to higher overall pump efficiency. However, the manner in which these positive effects are seen differs between graphite and CNTs and CNFs, and the results suggests that graphite and CNTs may be more beneficial as an additive at lower pressures and CNFs may be more effective at higher pressures. From a qualitative perspective, graphite and CNTs do not appear to degrade when run through the gear pump, while scission may be occurring with the CNFs. However, the high degree of filterability of these additives is problematic and would need to be specifically addressed if they were to be used in an industrial application.

Though various mechanisms that produce these positive results have been proposed none have been conclusively proven. If this study were continued, there are a number of research actions that could help verify or disprove these hypotheses. One action would be to obtain ESEM images of the pump gears and housing walls both before and after running experiments with the nanoadditives. This would allow verification of the hypothesis that the additives adhere to the asperities of the metal surfaces. This procedure was never performed because the ESEM used in this study was not large enough to fit the pump gears and housing in

its holding chamber. Another research action would be to develop a method in which high speed images of the flow as it travels through the gears and pump housing could be obtained. This would require (at the least) that the pump housing be constructed of a transparent material. This may help to verify the roller-bearing effect that the tubes and fibers may possibly exhibit.

A recommended computational research action would be to use a simulation tool such as PumpLinx from Simerics. The flow could be simulated both with and without the nanoadditives, and a comparison of the gap clearances between the gears themselves and the gears and pump housing for each case could be produced. This would give further insight into the roller-bearing effect by which the nanoadditives may effectively reduce the paths through which internal leakage occurs. It would also be beneficial to test these additives in different sized pumps, different types of pumps, and in different hydraulic fluids to see if they produced similar effects.

Finally, it would be important to reduce the size and shape of the additives while maintaining performance in terms of increased efficiency. In particular, the particles would need to be small enough so that they are not filtered and do not make the liquid opaque, i.e. appear dirty. This would likely require an order of magnitude reduction in the length-scales of the particles, i.e. such that the longest dimension would be on the order of, or even less than, one micron.

## References

- [1] Manrig N. Measuring pump efficiency: uncertainty considerations. *Transactions of the ASME* 2005; 127: 280-284.
- [2] Kozlov Y. N, Polyakov Y. N, Kozlova G I, Medvedev V. D and Faidel G. I. A study of the operation of a gear pump on highly viscous polymer solutions, *Chemical and Petroleum Engineering*, 1973; 9: 329-332.
- [3] Hall J. H. Internal gear pumps—your second choice for thin liquids, *World Pumps*, 2005; 2005 (469): 32-37.
- [4] Durfee W, Sun Z. *Fluid power system dynamics*. University of Minnesota, 2009.
- [5] Bielmeier E, Bartholomae I, Neveu CD. Measurement of the temporary shear stability of lubricants in a gear pump. *Tribotest Journal* 1999; 193 (6): 193-204.
- [6] Dearn R. The fine art of gear pump selection and operation. *World Pumps* 2001; 2001 (417): 38-40.
- [7] Jing B, Yang L, Lu S. The research of contaminant abrasion on external gear pump. *Proceedings of the 2009 Chinese Control and Decision Conference (CCDC2009)*, Guilin (China): IEEE, 2009; p. 3090–3.
- [8] Bhushan B. *Principles and applications of tribology*. New York: John Wiley & Sons; 1999.
- [9] Williams J. *Engineering tribology*. Cambridge: Cambridge University Press; 2005.
- [10] Blau P. *Friction Science and Technology*. 2<sup>nd</sup> ed. Boca Raton FL: CRC Press; 2009.
- [11] Lee C-G, Hwang Y-J, Choi Y-M, Lee J-K, Choi C, Oh J-M. A study of the tribological characteristics of graphite nano lubricants. *International Journal of Precision Engineering and Manufacturing* 2009; 10 (1): 85-90.
- [12] Yang Y, Zhang ZG, Grulke EA, Anderson WB and Wu G. Heat transfer properties of nanoparticle-in-fluid dispersions (nanofluids) in laminar flow, *Int. J. Heat Mass Trans.* 2005;48 (6): 1107–1116.
- [13] Lau K, Hui D. The revolutionary creation of new advanced materials-carbon nanotube composites. *Composites: Part B* 2002; 33: 263-277.
- [14] Ozkan T, Naraghi M, Chasiotis I. Mechanical properties of vapor grown carbon nanofibers. *Carbon* 2010; 48: 239-244.
- [15] Paffoni B. *Proc. Instn Mech. Engrs Vol. 217 Part G: J. Aerospace Engineering* 2003.
- [16] Wedeven LD, Bourdoulous R. Hydraulic gear pump failure analysis and tribology simulation. In: Totten GE, Wills DK, Feldmann DG, editors. *Hydraulic failure analysis fluids components and system effects*, West Conshohocken: American Society for Testing Materials; 2001, p. 105–119.
- [17] Veronesi P, Sola R, Poli G. Electroless Ni coatings for the improvement of wear resistance of bearings for lightweight rotary gear pumps, *International Journal of Surface Science and Engineering* 2008; 2(3/4): 190-201.
- [18] Buckley DH, Brainard WA. *Carbon*, 1975; 13(6): 501-508.
- [19] Lu HF, Fei B, Xin JH, Wang RH, Li L, Guan WC. Synthesis and lubricating performance of a carbon nanotube seeded miniemulsion, *Carbon* 2007; 45: 936–942.